HAL
open science

Mixotrophic growth of the extremophile galdieria sulphuraria reveals the flexibility of its carbon assimilation metabolism

Gilles Curien, Dagmar Lyska, Erika Guglielmino, Phillip Westhoff, Janina Janetzko, Marianne Tardif, Clément Hallopeau, Sabine Brugière, Davide Dal Bo, Johan Decelle, et al.

▶ **To cite this version:**

HAL Id: hal-03193983
https://hal.science/hal-03193983

Submitted on 9 Apr 2021

1 **MIXOTROPHIC GROWTH OF THE EXTREMOPHILE *GALDIERIA***
2 ***SULPHURARIA* REVEALS THE FLEXIBILITY OF ITS CARBON**
3 **ASSIMILATION METABOLISM**
4

5 Gilles Curien[1]*, Dagmar Lyska[2], Erika Guglielmino[1], Phillip Westhoff[2], Janina

6 Janetzko[2], Marianne Tardif[3], Clément Hallopeau[1], Sabine Brugière[3], Davide Dal

7 Bo[1], Johan Decelle[1], Benoit Gallet[4], Denis Falconet[1], Michele Carone[5], Claire

8 Remacle[5], Myriam Ferro[3], Andreas P.M. Weber[2], Giovanni Finazzi[1]

9

10 [1]Laboratoire de Physiologie Cellulaire et Végétale. Univ. Grenoble Alpes, CNRS,

11 CEA, INRAe, 38054 Grenoble Cedex 9, France

12 [2]Institute of Plant Biochemistry, Cluster of Excellence on Plant Sciences

13 (CEPLAS), Heinrich Heine University, 40225 Düsseldorf, Germany

14 [3]EdyP Laboratoire Biologie à Grande Echelle. Univ. Grenoble Alpes, CEA, Inserm,

15 BGE U1038, 38054 Grenoble Cedex 9, France

16 [4]Institut de Biologie Structurale, Univ. Grenoble Alpes, CNRS, CEA, 71 Avenue

17 des Martyrs, 38044 Grenoble, France

18 [5]Genetics and Physiology of microalgae, InBios/Phytosystems Research Unit,

19 University of Liege, 4000, Belgium

20 *Corresponding author: Gilles Curien, phone: +33 4 38782509, email**:**

21 gilles.curien@cea.fr

22 ORCID numbers:
23 Gilles Curien: 0000-0002-5361-2399
24 Dagmar Lyska: 0000-0002-9175-6334
25 Marianne Tardif: 0000-0003-4438-8281
26 Clément Hallopeau : 0000-0002-0692-2407
27 Sabine Brugière : 0000-0002-0757-0968
28 Johann Decelle: 0000-0002-4343-8358
29 Benoit Gallet: 0000-0001-8758-7681
30 Denis Falconet: 0000-0001-8182-1182
31 Michel Carone: 0000-0002-5561-0792
32 Claire Remacle: 0000-0002-5016-9547
33 Myriam Ferro: 0000-0002-4222-6847
34 Andreas P.M. Weber: 0000-0003-0970-4672
35 Giovanni Finazzi: 0000-0003-0597-7075

36 total words count: 5225
37 words count for Introduction: 755.
38 words count for Material and methods: 1363

39 words count for Results: 2048
40 words count for Discussion: 1059
41 5 figures (all in color)
42 1 supporting information file (with 12 figures)
43 3 supporting datasets
44
45
46

47

Summary

- *Galdieria sulphuraria* is a cosmopolitan microalga found in volcanic hot springs and calderas. It grows at low pH in photoautotrophic (use of light as a source of energy) or heterotrophic (respiration as a source of energy) conditions, using an unusually broad range of organic carbon sources. Previous data suggested that *G. sulphuraria* cannot grow mixotrophically (simultaneously exploiting light and organic carbon as energy sources), its photosynthetic machinery being repressed by organic carbon.
- Here, we show that *G. sulphuraria* SAG21.92 thrives in photoautotrophy, heterotrophy and mixotrophy. By comparing growth, biomass production, photosynthetic and respiratory performances in these three trophic modes, we show that addition of organic carbon to cultures (mixotrophy) relieves inorganic carbon limitation of photosynthesis thanks to increased CO_2 supply through respiration. This synergistic effect is lost when inorganic carbon limitation is artificially overcome by saturating photosynthesis with added external CO_2.
- Proteomic and metabolic profiling corroborates this conclusion suggesting that mixotrophy is an opportunistic mechanism to increase intracellular CO_2 concentration under physiological conditions, boosting photosynthesis by enhancing the carboxylation activity of Rubisco and decreasing photorespiration.
- We discuss possible implications of these findings for the ecological success of Galdieria in extreme environments and for biotechnological applications.

72

75

76

Introduction

The unicellular red alga *Galdieria sulphuraria* belongs to the Cyanidiophyceae, a class that includes five species often flourishing in different extreme environments (Merola *et al.*, 1981; Gross *et al.*, 1998; Gross & Oesterhelt, 1999; Oesterhelt *et al.*, 2007). From a phylogenetic perspective, plastids of the red algae gave rise to the complex plastids of, *e.g.*, diatoms via secondary endosymbiosis (Yoon *et al.*, 2002; Bhattacharya *et al.*, 2003; Yoon *et al.*, 2004). Like other members of this class (Doemel & Brock, 1971; Reeb & Bhattacharya, 2010) *G. sulphuraria* has an extremophile lifestyle, withstanding low pH (pH optimum at 2) and elevated temperatures (up to 56°C). It thrives in soils and forms biomats on rocks surrounding hot springs, fumaroles, or acid mining sites and even on burning coal spoil heaps (Moreira *et al.*, 1994; Gross *et al.*, 1998; Castenholz & McDermott, 2010; Barcyté *et al.*, 2018). Some mesophilic species have been isolated from environments with moderate temperatures and/ or a neutral pH (Gross, W. *et al.*, 2002; Yoon *et al.*, 2006; Azúa-Bustos *et al.*, 2009; Iovinella *et al.*, 2018). Genome analysis (Barbier *et al.*, 2005; Schonknecht *et al.*, 2013; Rossoni *et al.*, 2019a) has pinpointed a very high metabolic flexibility of this alga, which is confirmed by its ability to grow in photoautotrophy (exclusive use of light as an energy source) and heterotrophy (organic carbon respiration of more than 50 different substrates, (Gross & Schnarrenberger, 1995)). This capacity, along with the peculiar pH optimum for growth, allow *G. sulphuraria* to be cultivated in open ponds containing organic matter, overcoming other microorganisms, considered as contaminants in this case. Given these advantages for large-scale cultivation, *G. sulphuraria* is considered an emerging system for biotechnology applications (Schmidt *et al.*, 2005; Henkanatte-Gedera *et al.*, 2017; Cizkova *et al.*, 2019).

The relationship between photosynthesis and glycolysis/respiration in higher plants and microalgae is complex (Avelange *et al.*, 1988; Kromer *et al.*, 1988; Gemel & Randall, 1992; Pärnik & Keerberg, 1995; Hoefnagel *et al.*, 1998; Tcherkez *et al.*, 2008). Photosynthesis/glycolysis/respiration interactions are prone to perturbation by mixotrophy, in which external organic carbon often interferes with carbon flow between chloroplasts, the cytosol and mitochondria. Several

109 green microalgae are capable of mixotrophic growth (Combres *et al.*, 1994; Wan
110 *et al.*, 2011; Johnson & Alric, 2012; Cecchin *et al.*, 2018). While mixotrophy has
111 always beneficial consequences on respiration, its effects on photosynthesis differ
112 depending on the microalga considered: enhancement of photosynthesis was
113 reported in one case (*Ettlia oleoabundans*, (Ferroni *et al.*, 2018)), while in other
114 algae, including the diatoms *Phaeodactylum tricornutum* (Liu *et al.*, 2009; Villanova
115 *et al.*, 2017) and *Nannochloropsis (Fang et al., 2004; Xu et al., 2004)*
116 photosynthesis was unaffected. Decreased photosynthetic activity in mixotrophy
117 has been reported in *Chlorella vulgaris* (Martinez & Orus, 1991; Cecchin *et al.*,
118 2018) and *Chlamydomonas reinhardtii* where the Carbon Concentrating
119 Mechanism (CCM, (Bogaert *et al.*, 2019)) and the light harvesting capacity
120 (Perrineau *et al.*, 2014) is decreased by acetate along with the enhancement of
121 respiration. While it has been reported that *G. sulphuraria* 074G could grow in the
122 simultaneous presence of light and a carbon source, heterotrophy seemed to
123 prevail in these conditions, as no photosynthetic O_2 production could be measured
124 in the presence of glucose (Oesterhelt *et al.*, 2007).
125 Here, we show instead that photosynthesis and carbon metabolism (glycolysis and
126 respiration) operate simultaneously in *Galdieria sulphuraria* SAG21.92 (a close
127 relative of the 074G strain) under mixotrophic conditions, provided that the
128 temperature conditions are kept close to the ones experienced by this alga in its
129 natural environment. We show that performances in mixotrophy, exemplified by
130 photosynthetic activity and biomass production, actually exceed the sum of the
131 heterotrophic and photoautotrophic yields under limiting inorganic carbon. This
132 synergistic effect stems from a stimulation of photosynthesis by CO_2 of respiratory
133 origin, which overcomes the limitation to the Calvin-Benson-Bassham cycle and
134 suppresses photorespiration.
135 Limitation originates from the very low inorganic carbon concentration available in
136 acidic conditions (pH 2) that constitute the alga's natural growth environment.
137 Notably, under these conditions, inorganic carbon is almost exclusively available
138 as dissolved CO_2 (around 10 µM) while soluble bicarbonate is virtually absent.
139 Consistent with this hypothesis, the synergistic effect of 'light' and 'dark' energetic

140 metabolisms is sensitive to respiration inhibitors and is lost upon addition of

141 exogenous CO_2, which outcompetes endogenous CO_2 of respiratory origin in

142 relieving inorganic carbon limitation of the Calvin-Benson-Bassham cycle. We

143 conclude that mixotrophy constitutes an efficient mechanism to increase

144 intracellular CO_2 concentration under physiological conditions, allowing *G.*

145 *sulphuraria* to successfully exploit all the energy resources available for growth in

146 its rather challenging environment.

147

148 **Materials and Methods**

149

150 ***Strains, growth and media composition***

151 *Galdieria sulphuraria* SAG21.92 and 074G were obtained from the Culture

152 Collection of Algae at Göttingen University (SAG) and were grown in sterile 2xGS

153 modified Allen medium, pH 2.0, containing 20 mM of $NaNO_3$, and 5 mM of

154 inorganic phosphate (K_2HPO_4 and KH_2PO_4 in a 2/1 ratio (Allen, 1959)) at 42°C

155 without or with organic substrates as indicated in the text. The concentration of

156 organic substrates was selected on the basis of data reported in literature

157 (Oesterhelt *et al.*, 2007). More precisely, glucose was employed at the

158 concentration of 25 mM, as in (Oesterhelt *et al.*, 2007). The concentration of all the

159 other organic compounds was adjusted to reach the same carbon atom

160 concentration (150 mM). *G. sulphuraria* was grown either in 250 mL flasks (50 mL

161 culture volume), in an incubator (Infors, Switzerland, continuous light, 30 µmol

162 photons m^{-2} s^{-1}, 42°C, 100 rpm) or in a photobioreactor (Multicultivator, Photon

163 System Instruments, Czech Republic). Inside the multicultivator, cells were

164 provided with air or CO_2-enriched air by active bubbling (see Methods S1).

165 Moreover, the incident light intensity was adjusted daily to maintain constant

166 transmitted light through the culture (see Results). This 'luminostat' regime

167 ensures maximal absorption of light without allowing a dark zone to develop inside

168 the photobioreactor (Cuaresma *et al.*, 2011). Growth was monitored daily by cell

169 counting with a LUNA cell counter (Logos Biosystems, Inc. USA). Sorbitol

170 consumption was measured using the D-Sorbitol/Xylitol assay kit (Megazyme).

171

172 ***Cell fresh weight and dry weight quantification***

173 Cell pellet was resuspended in a small volume of water and centrifuged in pre-

174 weighed Eppendorf tubes and pellet was weighed. For dry weight determination

175 fresh cells pellets were dried for three days at 60°C, weighed and expressed as

176 $g.L^{-1}$.

177

178 ***Clark electrode oxygen measurements***

179 Oxygen exchanges in solution were measured with a Clark-type electrode

180 (Hansatech Instruments, UK) at 42°C. Respiration and gross photosynthesis were

181 quantified by measuring the slope of O_2 changes in the dark and under light

182 exposure, respectively. Net photosynthesis was calculated assuming O_2

183 consumption by the mitochondrion in the light is identical to that in the dark (Net

184 photosynthesis = $v_{O2light}$ +$|v_{O2dark}|$).

185

186 ***Photophysiology measurements***

187 Photosynthetic parameters were derived from quantification of chlorophyll

188 fluorescence emission by cultures within the multicultivator. To this aim, we

189 employed a custom-made fluorescence imaging system based on a previously

190 published setup (Johnson *et al.*, 2009) modified as described in Methods S1. The

191 photosynthetic electron transfer rate, ETR (a proxy of the carbon assimilation

192 capacity (Maxwell & Johnson, 2000)) was calculated as (Fm'-Fs)/Fm'*PFD, where

193 Fm' and Fs are the fluorescence intensities measured after exposure to a

194 saturating pulse and in steady state, respectively, in light-acclimated cells and PFD

195 (Photosynthetic Flux Density) is the incident light intensity, measured in µmol

196 photons m^{-2} s^{-1}. The cells were allowed to reach steady state fluorescence

197 emissions at each intensity (5-10 minutes of light exposure depending on the

198 intensity) before increasing the photon flux.

199

200 ***Biochemistry and Proteomic analysis***

201 Western blot analysis was performed on cells grown for 7 days in the indicated

202 conditions. Cells (10^9 cells) were broken with a Precellys homogenizer (Bertin,

203   France), through three cycles of 30 seconds at 10,000 rpm separated by a 30-
204   seconds interval. Total protein extracts were analyzed by immunoblotting with an
205   anti- RuBisCO antibody (Agrisera, Sweden). An antibody against the β subunit of
206   the ATPsynthase complex (Agrisera, Sweden) was used as a loading control. 10
207   μg of protein was loaded per well.

208   For proteomic analysis, algae were cultivated under the three conditions
209   photoautotrophy, mixotrophy and heterotrophy in parallel in the same cultivator.
210   Three multicultivator experiments were carried out one week apart and constituted
211   the three independent biological replicates. Cells were collected on day 7 (*i.e.* 4
212   days after addition of 25 mM D-sorbitol to mixotrophic and heterotrophic cultures).
213   Proteins from whole cell extracts (40 μg each) were solubilized in Laemmli buffer
214   before being stacked in the top of a 4–12% NuPAGE gel (Life Technologies, US),
215   stained with R-250 Coomassie blue (Bio-Rad, US) and in-gel digested using
216   modified trypsin (sequencing grade, Promega, US) as previously described
217   (Bouchnak *et al.*, 2019). Resulting peptides were analyzed by online
218   nanoLC-MS/MS (Ultimate 3,000 RSLCnano coupled to Q-Exactive HF, Thermo
219   Fisher Scientific, US) using a 200-min gradient. Peptides and proteins were
220   identified using Mascot (version 2.6.0, Matrix Science). Spectra were searched
221   against Uniprot (*G. sulphuraria* taxonomy, July 2019 version, 7347 sequences)
222   concomitantly with a home-made list of contaminants frequently observed in
223   proteomics analyses (trypsins and keratins, 250 sequences).

224

225   The Proline software (Bouyssie *et al.*, 2020) was used to filter the results
226   (conservation of rank 1 peptides, peptide identification FDR < 1% as calculated on
227   peptide scores by employing the reverse database strategy, minimum peptide
228   score of 25, and minimum of 1 specific peptide per identified protein group). Proline
229   was then used to extract the MS1-based intensities values of protein groups from
230   unique peptides. Proteins identified in the reverse and contaminant databases (i.e.
231   trypsin or keratin), and proteins identified with only 1 peptide with a score <40 were
232   further discarded from the list. Proteins identified in only one or two conditions were
233   kept for analysis without statistical treatment. Proteins identified in all three

234 conditions were submitted to statistical differential analysis using ProStaR
235 (Wieczorek *et al.*, 2017; Wieczorek *et al.*, 2019). Detailed procedures are
236 described in Methods S1.

237

238 ***Metabolite extraction and analysis***

239 Cells grown in a multicultivator were harvested at day 5 by centrifugation (4°C, 5
240 min and 3,000 rcf), washed with ice-cold 0.9 % (w/v) NaCl, snap frozen in liquid
241 nitrogen, and lyophilized overnight. Cells (5 x 10^8) were disrupted in a Mixer Mill
242 (MM 400, Retsch GmbH, Haan, Germany) for 60 seconds at 30 Hz using metal
243 beads and 500 µL of ice-cold chloroform and methanol (1:2.3 ratio; containing 5
244 µM Ribitol and 2,4-Dimethylphenylalanine (both Sigma-Aldrich, Munich, Germany)
245 as internal standards) with another round of shaking in the Mixer Mill. After a 2 h
246 incubation at -20°C, 400 µL of ice-cold deionized water (Milli Q, Merck Chemicals
247 GmbH, Darmstadt, Germany) were added to induce phase separation. The
248 samples were vortexed and centrifuged for 5 min at 4°C and 16,000 rcf. The
249 aqueous phase was transferred to a new reaction tube and the organic phase was
250 re-extracted with 400 µL of ice-cold deionized water. Aqueous phases of each
251 sample were combined and lyophilized overnight. After resuspension in 500 µL of
252 50% methanol 50 µL were dried in a glass inlet for analysis by GC-MS and IC-MS.

253

254 For GC-MS analysis the samples were prepared and analyzed as described (Gu
255 *et al.*, 2012) and (Shim *et al.*, 2020). Identification of metabolites was performed
256 with MassHunter Qualitative (v b08.00, Agilent Technologies) by comparing
257 spectra to the NIST14 Mass Spectral Library (https://www.nist.gov/srd/nist-
258 standard-reference-database-1a-v14) and to a quality control sample containing
259 all target compounds. Peaks were integrated using MassHunter Quantitative (v
260 b08.00, Agilent Technologies). For relative quantification, all metabolite peak
261 areas were normalized to the peak area of the internal standard ribitol.

262 For IC-MS a combination of a Dionex ICS-6000 HPIC and a high field Thermo
263 Scientific Q Exactive Plus quadrupole-Orbitrap mass spectrometer following the
264 method described in (Schwaiger et al., 2017) and in Methods S1. Data Analysis

265   was conducted using Compound Discoverer (version 3.1, Thermo Scientific).

266   Setting parameters for the untargeted metabolomics workflow and peak annotation

267   criteria are described in Methods S1.

268

269   ***Labelling experiments with ^{13}C-glucose***

270   Cells were cultivated in 250 mL Erlenmeyer flasks (50 mL culture volume) for four

271   days under continuous light at 60 μmol m^{-2} s^{-1}, 40 °C and ambient air (0.04% CO_2).

272   U-^{13}C$_6$-glucose (Cambridge Isotope Laboratories Inc, Tewksbury, Massachusetts)

273   was added at day 4 in a final concentration of 25 mM and the irradiance was

274   increased to 100 μmol m^{-2} s^{-1} either under ambient or elevated (2%) CO_2

275   conditions.

276   1-2.5 x10^8 cells were harvested 1, 4, 12, 24, 36, 48 and 60 hours after glucose

277   addition as described above. Metabolites were extracted and measured by IC-MS

278   as described above.

279   Data analysis was conducted with Compound Discoverer (version 3.1, Thermo

280   Scientific) and the standard workflow for stable isotope labelling from Compound

281   Discoverer was chosen. The default settings, which are 5 ppm mass tolerance, 30

282   % intensity tolerance and 0.1 % intensity threshold for isotope pattern matching

283   were used and the maximum exchange rate was set to 95%.

284

285

286   **Results**

287

288   ***G. sulphuraria metabolises several organic substrates.***

289   Previous work (Oesterhelt *et al.*, 2007) has suggested that *G. sulphuraria* is unable

290   to grow mixotrophically in the presence of light plus organic carbon but rather

291   alternates between heterotrophy (in the presence of an external source of organic

292   carbon) and phototrophy (upon inorganic carbon consumption). This conclusion

293   was based on experiments carried out at 25°C, *i.e*. a temperature that is far from

294   the physiological optimum of this alga (above 40°C), and therefore decreases

295   photosynthetic performances (Doemel & Brock, 1971; Ford, 1979; Rossoni *et al.*,

296   2019b; Rossoni & Weber, 2019). Thus, we decided to reinvestigate the possible

297 occurrence of mixotrophy under conditions that resemble natural growth conditions

298 (42°C, pH 2.0) in which *G. sulphuraria* displays maximum photosynthetic capacity.

299 First, we sought compounds that could improve algal growth in presence of light.

300 We found that several hexoses, disaccharides and pentoses, but also some

301 polyols and amino acids (L-alanine, L-glutamate) were able to boost *G.*

302 *sulphuraria*'s growth when compared to strict photoautotrophic conditions (Fig.

303 S1). Conversely, some organic acids (malic and citric acid) and amino acids (L-

304 aspartate, L-leucine, L-valine, L-isoleucine, L-asparagine) had either no effect or

305 led to a growth inhibition when compared to photoautotrophic conditions. Acetic

306 acid was lethal to the cells. Compound concentrations were 25 mM, i.e., the same

307 value employed in the study by Oesterhelt and colleagues. In the case of

308 disaccharides, we reduced the concentration by a factor of two, to keep the overall

309 carbon atoms concentration constant.

310 Based on these results, we focused on sorbitol, a compound that boosts growth in

311 the dark without inducing a significant loss of photosynthetic pigments (Gross &

312 Schnarrenberger, 1995). We confirmed that sorbitol was able to sustain cell

313 division in the dark (Fig. 1), but its effect on growth was largely enhanced by a

314 concomitant exposure to light. The final dry weight and number of cells collected

315 at the end of the exponential phase in the light plus carbon condition (orange

316 symbols) exceeded the sum of cells obtained in the heterotrophic (black) plus the

317 photoautotrophic (green) conditions (Fig. 1a-b). This finding indicates that *G.*

318 *sulphuraria* is not only able to perform true mixotrophy under high temperature,

319 dim light and presence of external organic carbon sources, but that this trophic

320 mode is highly beneficial for its growth capacity. We obtained similar effects

321 replacing sorbitol with a monosaccharide (glucose) and a disaccharide

322 (saccharose) (Fig. S2).

323

324 ***Respiration boosts photosynthesis in mixotrophic Galdieria cells.***

325 To further characterize the consequences of mixotrophy in *G. sulphuraria*, we

326 transferred half of the cells grown in mixotrophy for five days (Fig. 1) to

327 heterotrophic condition and monitored growth of the four samples

11

328   (photoautotrophic: green, heterotrophic: black, mixotrophic: orange and

329   mixotrophic transferred to heterotrophy: grey) for another five days. While the

330   mixotrophic cells   continued to display a higher growth capacity than the

331   heterotrophic plus photoautotrophic ones, the mixotrophic cells transferred to the

332   dark (grey) slowly reached the same cell density (Fig. 1a) and dry weight (Fig. 1b)

333   as the heterotrophic culture, *i.e.*, they lost the benefits provided by the

334   simultaneous exposure to light and organic carbon within a few days. We conclude

335   therefore that mixotrophy promotes a synergistic interaction between light and dark

336   energy metabolisms, which slowly disappears when the light supply is halted.

337   In the experiments described above, photoautotrophic growth was most likely

338   limited by the low light intensity (30 µmol photons m^{-2} s^{-1}), which was kept constant

339   during growth, and therefore rapidly became limiting for photosynthesis when the

340   cell concentration was increased in the flasks. Gas diffusion could also be limiting

341   in flasks. Therefore, we repeated experiments in a photobioreactor (Multicultivator,

342   PSI, Czeck Republic, Fig. S3), where air bubbling ensured a more efficient gas

343   delivery to the algae. Moreover, the intensity of the incident light was progressively

344   increased in this setup to maintain a linear relationship between the cell number

345   and the absorption. We reproduced the improvement of biomass productivity in

346   mixotrophy with the photobioreactor (Fig. 2), where we could monitor biomass

347   production and photosynthetic performances on actively growing cells using a

348   custom-built fluorescence imaging setup to monitor photosynthesis via the electron

349   transfer rate (ETR) parameter (Maxwell & Johnson, 2000) (Fig. S3).

350   The ETR in the photoautotrophic cultures was lower than in mixotrophic ones (Fig.

351   2a). The difference was larger during the first days of culturing (Fig. S4, days 4

352   and 5, i.e. the first and second day after sorbitol addition), and then photosynthesis

353   progressively diminished in the mixotrophic cells (Fig. S4, days 6 and 7, i.e. the

354   third and fourth day of mixotrophy), where we also observed a large variability in

355   the photosynthetic capacity (Fig. S4, day 7). We ascribe this variability to a

356   differential consumption of sorbitol, and therefore of the mixotrophic synergistic

357   effect, in the various samples. Consistent with this hypothesis, enhancement of

358   photosynthesis was re-established in mixotrophic cultures, provided that sorbitol,

359　nearly exhausted after four days (Fig. S5, day 7) was added again to the growth

360　medium (Fig. S6).

361　To explain the synergistic effect of mixotrophy, we reasoned that photosynthesis

362　could be limited by the availability of inorganic carbon in photoautotrophic cells.

363　The latter is present only as CO_2 and at very low concentration (10 µM, (Gross *et*

364　*al.*, 1998)) at ambient air in *G. sulphuraria*'s cultures, due to the acidic pH (pH 2).

365　Mixotrophy could alleviate this limitation by providing extra CO_2 of mitochondrial

366　origin via enhanced respiration (Fig. 2c, Fig. S7). We tested this hypothesis by two

367　approaches. First, we poisoned mixotrophic and photoautotrophic cultures with

368　myxothiazol and SHAM, known inhibitors of the cyanide sensitive and insensitive

369　respiratory　pathways,　respectively,　and　measured　consequences　on

370　photosynthetic activity. Addition of these inhibitors completely abolished the

371　enhancement of photosynthetic activity and of biomass productivity by mixotrophy

372　(Fig. 2d-f). Next, we increased the CO_2 availability to the cells in mixotrophic

373　cultures, to outcompete endogenous CO_2 of respiratory origin with an excess of

374　exogenous inorganic carbon. As a prerequisite for this experiment, we calibrated

375　the　CO_2　requirement　for　optimum　photosynthesis　in　our　growth　conditions

376　(transmitted light of 10 µmol photons m^{-2} s^{-1}). We found that photoautotrophic

377　growth was increased by CO_2 up to a concentration of 2% CO_2 (Fig. S8a), the

378　apparent affinity for CO_2 being 0.5 % ca. Upon addition of external CO_2, the

379　photosynthetic capacity in photoautotrophic conditions increased and the biomass

380　produced in heterotrophic plus photoautotrophic conditions became equal to that

381　observed in mixotrophy (Fig. 2g-i). Overall, these data indicate that the synergy

382　between respiration and photosynthesis is lost when the respiration is inhibited or

383　when　the　photosynthesis　becomes　saturated　with　externally　supplied　CO_2.

384　Moreover, we hypothesize that photorespiration should be decreased to very low

385　rates at saturating CO_2, possibly contributing to the gain in biomass productivity at

386　high CO_2 concentrations. In these experiments, we also observed that the amount

387　of biomass produced by phototrophic cells supplemented with air was the same

388　irrespective of the light intensity employed (Fig S8b). Conversely, biomass

389　production could be increased by increasing the light intensity in both phototrophic

390   cells supplemented with 0.5% CO2 (Fig S8c) or in mixotrophic cells (Fig S8d).

391   These findings are fully consistent with the hypothesis that photosynthesis is CO_2

392   limited in air, and that this limitation can be alleviated by endogenous (mixotrophy)

393   or exogenous CO_2.

394

395   ***Metabolic acclimation to mixotrophy in G. sulphuraria.***

396   The observation that mixotrophy enhances photosynthesis to a similar level as

397   upon addition of external CO_2 to *G. sulphuraria*, suggests that mixotrophy behaves

398   as a strategy to traffic CO_2 from the mitochondria to the plastid, allowing this alga

399   to successfully exploit all the energy resources available for growth and to

400   minimize energy loss through photorespiration.

401   To substantiate this hypothesis, we performed a complete survey of the metabolic

402   changes between the three trophic lifestyles, and relate these changes to

403   modifications in the cell proteome. We found that photosynthetic proteins

404   (complexes of the electron transfer chain, enzymes of the Calvin-Benson-

405   Bassham cycle and transporters involved in triose phosphate export) were

406   downregulated in mixotrophic conditions compared to photoautotrophic conditions

407   (Fig. 3), in agreement with previous suggestions (Gross & Schnarrenberger, 1995;

408   Oesterhelt *et al.*, 2007). Conversely, respiratory protein levels remained relatively

409   constant in the three conditions. This observation (photosynthetic activity is

410   enhanced in mixotrophy despite the downregulation of the photosynthetic

411   machinery) fully supports the conclusion that intracellular increase in CO_2 due to

412   enhanced respiratory activity more than compensates for the decrease in Rubisco

413   (see also Fig. S9).

414   In line with the hypothesis that mixotrophy channels CO_2 from respiration to

415   photosynthesis, proteomic analysis indicates that all the enzymes involved in

416   photorespiration (phosphoglycolate phosphatase, glycolate oxidase, serine-

417   glyoxylate aminotransferase, glycine decarboxylase, glycine/serine

418   hydroxymethyltransferase, hydroxypyruvate reductase, glycerate kinase) were

419   less abundant in mixotrophy. This is also true for Rubisco activase (Gasu_19410,

420   dataset S1-2), an enzyme that was shown to be important under low CO_2 in

421   *Chlamydomonas* (Pollock *et al.*, 2003). These findings are also corroborated by

422   metabolite analysis (Fig. 4a). The amounts of the oxygenation product of Rubisco,

423   2-phosphoglycolate are highest under photoautotrophic conditions, lower in

424   mixotrophic conditions, and very low in heterotrophic conditions. Glycine

425   accumulates, likely due to a higher reduction potential inside the mitochondrial

426   matrix under mixotrophic conditions, which will reduce the rate of oxidative

427   decarboxylation of glycine by glycine decarboxylase. Consequently, the glycine to

428   serine ratio was inverted compared to photoautotrophic conditions. The amounts

429   of glycerate and 3-phosphoglycerate under mixotrophic conditions are mimicking

430   those in heterotrophically grown cells (Fig. 4a).

431   Proteins involved in a putative C4-like carbon concentrating cycle (Rademacher *et*

432   *al.*, 2017) (Fig. 3, 4b) followed the same pattern as the photorespiratory enzymes.

433   Carbonic anhydrase and phosphoenolpyruvate carboxylase were more abundant

434   under photoautotrophic conditions than under mixotrophic or heterotrophic

435   conditions, and, in agreement with this finding, photoautotrophic cells also

436   contained higher amounts of phosphoenolpyruvate (PEP) than mixotrophic or

437   heterotrophic cells (Fig. 4b). The presence of this carbon concentrating cycle in

438   photoautotrophic conditions could be supported by increased steady-state levels

439   of phosphorylated C3 compounds, as suggested by the downregulation of

440   pyruvate kinases in phototrophy (PEP consumption might be decreased) and

441   strong induction of pyruvate ortho-phosphate dikinase (producing PEP). We

442   assume that oxaloacetate (OAA) under photoautotrophic conditions is

443   decarboxylated by PEP carboxykinase (PEPCK), and not after reduction into

444   malate by malate dehydrogenase and decarboxylation by mitochondrial malic

445   enzyme. This hypothesis is supported by the finding that mitochondrial malic

446   enzyme (ME) is strongly decreased in photoautotrophy (Fig. 3) and the malate pool

447   size is smaller under this condition than in mixo- or heterotrophy. We note that

448   decarboxylation by PEPCK (as compared to ME) is energy conserving and directly

449   yields PEP for a new round of carboxylation by PEP carboxylase.

450   While part of the increase in biomass production in mixotrophic conditions can be

451   attributed to the repression of photorespiration, other benefits of the mixotrophic

452   lifestyle may come from more carbon units being shuttled into anabolic pathways.

453   Indeed, we observed a general increase of metabolites of the oxidative pentose

454   phosphate pathway (Ribulose-5P, Sedoheptulose-7P) and nucleoside

455   triphosphates (ATP, GTP, UTP, CTP) as successor metabolites (Fig. 4c). The

456   amounts do not differ between autotrophic and heterotrophic cultures but are

457   clearly increased under mixotrophic conditions providing evidence for a higher flux

458   of carbon at least into purine and pyrimidine synthesis.

459   Labelling experiments using ^{13}C-labelled glucose, a sugar with similar effects on

460   cell growth and biomass production as sorbitol (Fig. S2), further support this notion.

461   We found a rapid incorporation of CO_2 from ^{13}C glucose into photosynthetic

462   metabolites, such as Ribulose1,5-bisphosphate (RuBP), Sedoheptulose 1,7-

463   bisphosphate (SBP), and 2-phosphoglycolate (2-PG) (Fig. 5). While RuBP also

464   occurs in the oxidative pentose phosphate pathway, SBP and 2-PG are

465   metabolites solely formed in the Calvin-Benson-Bassham cycle and can only carry

466   a label when $^{13}CO_2$ released by respiration is fixed. Incorporation of the label by

467   shuttling of carbon backbones from the cytosol into the chloroplast is unlikely since

468   the solute transporters in the *G. sulphuraria's* chloroplast envelope do not favor

469   the import of glycolytic intermediates under photosynthetic conditions (Linka *et al.*,

470   2008). The rate of incorporation of ^{13}C is much reduced when external CO_2 levels

471   are increased to 2%. Interestingly, the tricarboxylic acid cycle intermediate

472   succinate exhibits a similar pattern of delayed labelling under high CO_2 conditions

473   when compared to ambient air, indicating a slowed down glucose usage. Thus, the

474   delay of label incorporation into the Calvin-Benson-Bassham cycle intermediates

475   can be traced back to lower levels of labelled respiratory CO_2 under CO_2 saturated

476   conditions.

477

478   **Discussion**

479

480   At variance with a previous report (Oesterhelt *et al.*, 2007), *G. sulphuraria* cells are

481   capable of a true mixotrophy, when transferred from strictly photoautotrophic

482   conditions to a light and organic carbon regime, provided that the temperature

483   conditions are kept close to the ones experienced by this alga in its natural

484 environment. This is not only true for the *G. sulphuraria* SAG21.92 strain used
485 here, but also for *G. sulphuraria* 074G, *i.e.*, the strain used in the previous study
486 by Oesterhelt *et al.*, (2007) when tested in the presence of the same external
487 organic carbon sources employed here (See Fig. S10). Acclimation of the strictly
488 photoautotrophic Cyanidiophyceae *Cyanidioschyzon merolae* to suboptimal
489 growth temperatures of 25°C, led to massive rearrangements of the photosynthetic
490 apparatus and a lower photon-to-oxygen conversion rate when compared to cells
491 grown at 42°C (Nikolova *et al.*, 2017). Also, cultivation of *G. sulphuraria* at 25°C
492 led to a downregulation of transcripts encoding components of the photosynthetic
493 machinery (Rossoni *et al.*, 2019b). Therefore, cultivation at suboptimal
494 temperatures may not be in favor of high photosynthetic rates and drive
495 Cyanidiophyceae species capable of heterotrophic growth towards this trophic
496 state.
497 Mixotrophy deeply alters the carbon metabolism of *G. sulphuraria* cells. Under
498 photoautotrophic conditions, CO_2 is mainly concentrated by the PEPC/PEPCK
499 driven CCM (Rademacher *et al.*, 2017). This process is repressed in mixotrophy.
500 Moreover, enhanced respiration relieves the limitation of photosynthesis by
501 inorganic carbon, which is at a low concentration (µmolar range) in the acid growth
502 medium of this alga. We can quantify the extent of this process using the Clark
503 electrode (as in Fig S7) in a closed configuration, to avoid gas exchanges with the
504 atmosphere (representative traces in Fig S11a,c). In this case, the amount of O_2
505 produced by photosynthesis (32.3 ± 7.5 µM and 76.6 ± 2 µM in photoautrotrophy
506 and mixotrophy, respectively) is commensurate with the amount of CO_2 available
507 to Rubisco, *i.e.* the sum of respiratory CO_2 (22 ± 10.5 µM and 61 ± 1.5 µM
508 respectively, assuming a 1/1 stoichiometry with consumed O_2) plus the small CO_2
509 amount present in the medium (10 µM *ca* at pH 2) (Fig. S11c,d). These estimates
510 clearly indicate that respiration in mixotrophy sets the rate of photosynthesis under
511 limited CO_2 conditions. The proximity between mitochondria and chloroplasts
512 (highlighted in red and green, respectively, in Fig. S12) may favor this process,
513 facilitating intracellular gas exchange between the two cell organelles, as already
514 shown in the case of other microalgae (Lavergne, 1989).

515   At the same time, increased intracellular CO_2 concentration is expected to lower

516   the rate of photorespiration in mixotrophy. Although the Rubisco enzymes form

517   Cyanidiophyceae show some of the highest carboxylation specificities reported to

518   date (Sugawara *et al.*, 1999), photorespiration is expected to proceed at high rates

519   at the high temperatures and low CO_2 concentrations under which Galdieria grows.

520   Indeed, knockout of peroxisomal glycolate oxidase in the transformable

521   Cyanidiales alga *C. merolae* demonstrated that a functional photorespiratory

522   pathway is essential for survival of these algae under ambient CO_2 concentrations

523   (Rademacher *et al.*, 2016). The observed increase in the rate of photosynthesis

524   and gain of biomass under high CO_2 and mixotrophic conditions (25 ± 6 %, when

525   combining data from Fig. 1-2) is consistent with overcoming the expected loss of

526   biomass gain due to photorespiration under photoautotrophic conditions.

527   In conclusion, by bypassing the possible metabolic antagonism between

528   respiration and photosynthesis, *G. sulphuraria* can exploit the plethora of

529   transporters encoded by its genome (Schonknecht *et al.*, 2013; Rossoni *et al.*,

530   2019a) and import organic carbon available in its environment and to boost CO_2

531   availability for photosynthesis. While this phenomenon certainly exists in other

532   phototrophs (e.g. Rolland *et al.*, 1997), the capacity to enhance photosynthesis

533   with respiratory CO_2 when the latter process is increased by exogenous carbon

534   sources could be particularly relevant in *G. sulphuraria.* This alga thrives in an

535   extreme environment, where growth is limited by low pH, high temperature and

536   possibly light availability. Dissolved inorganic carbon is very low in this hot and

537   acidic milieu (in fact its concentration inversely correlates with the pH of different

538   collection sites in Yellowstone National Park) (Boyd *et al.*, 2012; Hamilton *et al.*,

539   2012) and its light-driven uptake is fairly low when compared to alkaline thermal

540   habitats. Conversely, the concentration of dissolved organic carbon can be

541   relatively high in the acidic hot springs (from 17 µM to 3 mM (Nye *et al.*, 2020)).

542   Values could become much higher when this alga proliferates in mats (Gross *et*

543   *al.*, 1998), where by-products of every group of microorganisms may serve as

544   "food" for other groups.

545   Based on these considerations, it is tempting to speculate that while
546   photosynthesis should allow cells to colonize new environments devoid of any
547   organic carbon source, the peculiar division mode of *G. sulphuraria* (formation of
548   endospores associated with the release in the media of the mother cell wall
549   remnants), may favor mixotrophy on a longer time scale. In the acidic conditions
550   where *G. sulphuraria* lives, this material is probably rapidly hydrolyzed, providing
551   an organic carbon source to the algae, along with other external sources for
552   dissolved organic carbon, like *e.g.* high-temperature acid-digested wood (Nye *et*
553   *al.*, 2020). Thanks to the abundance of transporters, this alga could outcompete
554   other microorganisms such as fungi, which are also found in these extreme
555   conditions, for growth. Thus, the coexistence of phototrophic, mixotrophic, and
556   heterotrophic lifestyles thanks to the subtle compromise between the activity of the
557   two energy-producing pathways (photosynthesis and respiration) would represent
558   a key element for fitness and explain the success of *G. sulphuraria* to thrive in its
559   extreme ecological niche. High fluctuations in the availability of dissolved organic
560   and inorganic carbon, light, temperature, etc. in these environments possibly
561   selected for the maintenance of a metabolic flexibility (Gross, 1999; Gross,
562   Wolfgang *et al.*, 2002; Ciniglia *et al.*, 2004; Cho *et al.*, 2020), which may have also
563   allowed Cyanidiales to invade more moderate habitats (Yoon *et al.*, 2006; Azúa-
564   Bustos *et al.*, 2009; Castenholz & McDermott, 2010) and to disperse over long
565   distances to geographically isolated extreme habitats (Rossoni *et al.*, 2019a).
566   The same metabolic flexibility opens interesting perspectives to exploit this alga
567   for biotechnology applications. *G. sulphuraria* has already been employed in the
568   fields of pigment/antioxidant production, bioremediation and bioenergy (Cizkova *et*
569   *al.*, 2019) and the possibility to exploit its lifestyle flexibility should be explored to
570   cultivate this alga in organic matter-rich open ponds without contamination by other
571   microorganisms.

572

573

574

575

Author Contributions
G.C., D.L., A.P.M.W. and G.F. designed research; G.C., D.L., E.G., P.W., J.J., C.H., S.B., D.D.B., J.D., B.G., D.F., M.C. and G.F. performed research; G.C., D.L., P.W., M.T., C.R., M.F., A.P.M.W. and G.F. analyzed data; G.C., D.L., A.P.M.W and G.F. wrote the paper.

Data availability

The original contributions presented in the study are included in the article and in the Supplementary information and supplementary dataset files. Further inquiries can be directed to the corresponding author

References

Allen GJ. 1959. Studies with *Cyanidium caldarium*, an anomalously pigmented chlorophyte. *Archiv für Mikrobiologie* **32**: S. 270-277.

Avelange MH, Thiéry JM, Sarrey F, Gans P, Rébeillé F. 1988. Mass-spectrometric determination of O_2 and CO_2 gas exchange in illuminated higher-plant cells. *Planta* **183**: 150-157.

Azúa-Bustos A, González-Silva C, Mancilla RA, Salas L, Palma RE, Wynne JJ, McKay CP, Vicuña R. 2009. Ancient photosynthetic eukaryote biofilms in an Atacama desert coastal cave. *Microbial Ecology* **58**(3): 485-496.

Barbier G, Oesterhelt C, Larson MD, Halgren RG, Wilkerson C, Garavito RM, Benning C, Weber APM. 2005. Comparative genomics of two closely related unicellular thermo-acidophilic red algae, Galdieria sulphuraria and *Cyanidioschyzon merolae*, reveals the molecular basis of the metabolic flexibility of *Galdieria sulphuraria* and significant differences in carbohydrate metabolism of both algae. *Plant Physiology* **137**(2): 460-474.

Barcyté D, Nedbalova L, Culka A, Kosek F, Jehlicka J. 2018. Burning coal spoil heaps as a new habitat for the extremophilic red alga *Galdieria sulphuraria*. *Fottea* **18**: 19-29.

Bhattacharya D, Yoon H, Hackett JD. 2003. Photosynthetic eukaryotes unite: endosymbiosis connects the dots. *Bioessays* **26**: 50–60.

Bogaert KA, Perez E, Rumin J, Giltay A, Carone M, Coosemans N, Radoux M, Eppe G, Levine RD, Remacle F, et al. 2019. Metabolic, physiological, and transcriptomics analysis of batch cultures of the green microalga Chlamydomonas grown on different acetate concentrations. *Cells* **8**(11), 1367.

Bouchnak I, Brugiere S, Moyet L, Le Gall S, Salvi D, Kuntz M, Tardif M, Rolland N. 2019. Unraveling hidden components of the chloroplast envelope proteome: Opportunities and limits of better MS sensitivity. *Mol & Cell Proteomics* **18**(7): 1285-1306.

Bouyssie D, Hesse AM, Mouton-Barbosa E, Rompais M, Macron C, Carapito C, de Peredo AG, Coute Y, Dupierris V, Burel A, et al. 2020. Proline: an efficient and user-friendly software suite for large-scale proteomics. *Bioinformatics* **36**(10): 3148-3155.

Boyd ES, Fecteau KM, Havig JR, Shock EL, Peters JW. 2012. Modeling the habitat range of phototrophs in Yellowstone National Park: toward the development of a comprehensive fitness landscape. *Front Microbiol* **3**. 221.

Castenholz RW, McDermott TR 2010. The Cyanidiales: Ecology, Biodiversity, and Biogeography. In: Seckbach J, Chapman DJ eds. *Red Algae in the Genomic Age*. Dordrecht: Springer Netherlands, 357-371.

Cecchin M, Benfatto S, Griggio F, Mori A, Cazzaniga S, Vitulo N, Delledonne M, Ballottari M. 2018. Molecular basis of autotrophic vs mixotrophic growth in *Chlorella sorokiniana*. *Scientific Reports* **8**, 6465.

Cho CH, Park SI, Ciniglia C, Yang EC, Graf L, Bhattacharya D, Yoon HS. 2020. Potential causes and consequences of rapid mitochondrial genome

evolution in thermoacidophilic Galdieria (Rhodophyta) (vol 20, 112, 2020). *BMC Evolutionary Biology* **20**, 112.

Ciniglia C, Yoon HS, Pollio A, Pinto G, Bhattacharya D. 2004. Hidden biodiversity of the extremophilic Cyanidiales red algae. *Molecular Ecology* **13**(7): 1827-1838.

Cizkova M, Vitova M, Zachleder V 2019. The red microalga galdieria as a promising organism for applications in biotechnology. In: Vítová M. ed. *Microalgae* - From Physiology to Application: IntechOpen: London, UK, pp. 105–122.

Combres C, Laliberte G, Reyssac JS, Delanoue J. 1994. Effect of acetate on growth and ammonium uptake in the microalga *Scenedesmus obliquus*. *Physiologia Plantarum* **91**(4): 729-734.

Cuaresma M, Janssen M, van den End EJ, Vilchez C, Wijffels RH. 2011. Luminostat operation: A tool to maximize microalgae photosynthetic efficiency in photobioreactors during the daily light cycle? *Bioresource Technol* **102**(17): 7871-7878.

Doemel WN, Brock TD. 1971. The physiological ecology of *Cyanidium caldarium*. *J Gen Microbiol* **67**: 17-32.

Fang X, Wei C, Cai ZL, Fan O. 2004. Effects of organic carbon sources on cell growth and eicosapentaenoic acid content of *Nannochloropsis sp*. *J Applied Phycol* **16**(6): 499-503.

Ferroni L, Giovanardi M, Poggioli M, Baldisserotto C, Pancaldi S. 2018. Enhanced photosynthetic linear electron flow in mixotrophic green microalga *Ettlia oleoabundans* UTEX 1185. *Plant Physiology and Biochemistry* **130**: 215-223.

Ford TW. 1979. Ribulose 1,5-bisphosphate carboxylase from the thermophilic, acidophilic alga, cyanidium-caldarium (geitler) - purification, characterization and thermostability of the enzyme. *Biochimica et Biophysica Acta (BBA) - Bioenergetics* **569**(2): 239-248.

Gemel J, Randall DD. 1992. Light regulation of leaf mitochondrial pyruvate-dehydrogenase complex - Role of photorespiratory carbon metabolism. *Plant Physiology* **100**(2): 908-914.

Gross C 1999. Revision of comparative traits for the acido-and thermophilic red algae Cyanidium and Galdieria. In: Seckbach J ed. *Enigmatic microorganisms and life in extreme environments* Dordrecht: Springer, 437-446.

Gross W, Küver J, Tischendorf G, Bouchaala N, Büsch W. 1998. Cryptoendolithic growth of the red alga *Galdieria sulphuraria* in volcanic areas. *European Journal of Phycology* **33**: 25-31.

Gross W, Oesterhelt C. 1999. Ecophysiological studies on the red alga *Galdieria sulphuraria* isolated from southwest iceland. *Plant Biol (Stuttgart, Germany)* **1**: 694-700.

Gross W, Oesterhelt C, Tischendorf G, Lederer F. 2002. Characterization of a non-thermophilic strain of the red algal genus Galdieria isolated from Soos (Czech Republic). *European Journal of Phycology* **37**: 477-483.

Gross W, Oesterhelt C, Tischendorf G, Lederer F. 2002. Characterization of a non-thermophilic strain of the red algal genus Galdieria isolated from Soos (Czech Republic). *European Journal of Phycology* **37**(3): 477-482.

Gross W, Schnarrenberger C. 1995. Heterotrophic growth of two strains of the acido-thermophilic red alga *Galdieria sulphuraria*. *Plant & Cell Physiology* **36**: 633-638.

Gu J, Weber K, Klemp E, Winters G, Franssen SU, Wienpahl I, Huylmans AK, Zecher K, Reusch TBH, Bornberg-Bauer E, et al. 2012. Identifying core features of adaptive metabolic mechanisms for chronic heat stress attenuation contributing to systems robustness. *Int Biol* **4**(5): 480-493.

Hamilton TL, Vogl K, Bryant DA, Boyd ES, Peters JW. 2012. Environmental constraints defining the distribution, composition, and evolution of chlorophototrophs in thermal features of Yellowstone National Park. *Geobiology* **10**(3): 236-249.

Henkanatte-Gedera SM, Selvaratnam T, Karbakhshravari M, Myint M, Nirmalakhandan N, Van Voorhies W, Lammers PJ. 2017. Removal of dissolved organic carbon and nutrients from urban wastewaters by *Galdieria sulphuraria*: Laboratory to field scale demonstration. *Algal Research-Biomass Biofuels and Bioproducts* **24**: 450-456.

Hoefnagel MHN, Atkin OK, Wiskich JT. 1998. Interdependence between chloroplasts and mitochondria in the light and the dark. *Biochim Biophys Acta-Bioenergetics* **1366**(3): 235-255.

Iovinella M, Eren A, Pinto G, Pollio A, Davis SJ, Cennamo P, Ciniglia C. 2018. Cryptic dispersal of Cyanidiophytina (Rhodophyta) in non-acidic environments from Turkey. *Extremophiles* **22**(5): 713-723.

Johnson X, Alric J. 2012. Interaction between starch breakdown, acetate assimilation, and photosynthetic cyclic electron flow in *Chlamydomonas reinhardtii*. *Journal of Biological Chemistry* **287**(31): 26445-26452.

Johnson X, Vandystadt G, Bujaldon S, Wollman FA, Dubois R, Roussel P, Alric J, Beal D. 2009. A new setup for in vivo fluorescence imaging of photosynthetic activity. *Photosynthesis Research* **102**(1): 85-93.

Kromer S, Stitt M, Heldt HW. 1988. Mitochondrial oxidative phosphorylation participating in photosynthetic metabolism of a leaf cell. *FEBS Letters* **226**: 352-356.

Lavergne J. 1989. Mitochondrial responses to intracellular pulses of photosynthetic oxygen. *Proc. Nat. Acad. Sci. USA* **86**(22): 8768-8772.

Linka M, Jamai A, Weber APM. 2008. Functional characterization of the plastidic phosphate translocator gene family from the thermo-acidophilic red alga *Galdieria sulphuraria* reveals specific adaptations of primary carbon partitioning in green plants and red Algae. *Plant Physiology* **148**(3): 1487-1496.

Liu XJ, Duan SS, Li AF, Xu N, Cai ZP, Hu ZX. 2009. Effects of organic carbon sources on growth, photosynthesis, and respiration of *Phaeodactylum tricornutum*. *J Applied Phycol* **21**(2): 239-246.

743 **Martinez F, Orus MI. 1991.** Interactions between glucose and inorganic carbon
744   metabolism in *Chlorella vulgaris* strain UAM-101. *Plant Physiology* **95**(4):
745   1150-1155.
746 **Maxwell K, Johnson GN. 2000.** Chlorophyll fluorescence - a practical guide.
747   *Journal of Experimental Botany* **51**(345): 659-668.
748 **Merola A, Castaldo R, De Luca P, Gambardella R, Musachio A, Taddei R.**
749   **1981.** Revision of *Cyanidium caldarium*. Three species of acidophilic algae.
750   *G. Bot. Ital.* **115**: 189–195.
751 **Moreira D, Lopezarchilla AI, Amils R, Marin I. 1994.** Characterization of 2 new
752   thermoacidophilic microalgae - genome organization and comparison with
753   *Galdieria sulphuraria*. *FEMS Microbiology Letters* **122**(1-2): 109-114.
754 **Nikolova D, Weber D, Scholz M, Bald T, Scharsack JP, Hippler M. 2017.**
755   Temperature-induced remodeling of the photosynthetic machinery tunes
756   photosynthesis in the thermophilic alga *Cyanidioschyzon merolae*. *Plant*
757   *Physiology* **174**(1): 35-46.
758 **Nye JJ, Shock EL, Hartnett HE. 2020.** A novel PARAFAC model for continental
759   hot springs reveals unique dissolved organic carbon compositions. *Organic*
760   *Geochemistry* **141**: 103964.
761 **Oesterhelt C, Schmalzlin E, Schmitt JM, Lokstein H. 2007.** Regulation of
762   photosynthesis in the unicellular acidophilic red alga *Galdieria sulphuraria*.
763   *Plant Journal* **51**(3): 500-511.
764 **Pärnik T, Keerberg O. 1995.** Decarboxylation of primary and end products of
765   photosynthesis at different oxygen concentrations. *Journal of Experimental*
766   *Botany* **46**: 1439-1477.
767 **Perrineau MM, Gross J, Zelzion E, Price DC, Levitan O, Boyd J, Bhattacharya**
768   **D. 2014.** Using natural selection to explore the adaptive potential of
769   *Chlamydomonas reinhardtii*. *PloS One* **9**(3), e92533.
770 **Pollock SV, Colombo SL, Prout DL, Godfrey AC, Moroney JV. 2003.** Rubisco
771   activase is required for optimal photosynthesis in the green alga
772   *Chlamydomonas reinhardtii* in a low-CO_2 atmosphere. *Plant Physiology*
773   **133**(4): 1854-1861.
774 **Rademacher N, Kern R, Fujiwara T, Mettler-Altmann T, Miyagishima SY,**
775   **Hagemann M, Eisenhut M, Weber APM. 2016.** Photorespiratory glycolate
776   oxidase is essential for the survival of the red alga *Cyanidioschyzon*
777   *merolae* under ambient CO_2 conditions. *Journal of Experimental Botany*
778   **67**(10): 3165-3175.
779 **Rademacher N, Wrobel TJ, Rossoni AW, Kurz S, Brautigam A, Weber APM,**
780   **Eisenhut M. 2017.** Transcriptional response of the extremophile red alga
781   *Cyanidioschyzon merolae* to changes in CO_2 concentrations. *Journal of*
782   *Plant Physiology* **217**: 49-56.
783 **Reeb V, Bhattacharya D. 2010.** The thermo-acidophilic Cyanidiophyceae
784   (Cyanidiales). In Red Algae in the Genomic Age. Seckbach J., Chapman D.
785   (eds) Cellular Origin, Life in Extreme Habitats and Astrobiology, vol 13.
786   Springer, Dordrecht. pp 409-426.
787 **Rolland N, Dorne AJ, Amoroso G, Sultemeyer DF, Joyard J, Rochaix JD.**
788   **1997.** Disruption of the plastid ycf10 open reading frame affects uptake of

inorganic carbon in the chloroplast of Chlamydomonas. *EMBO Journal* **16**(22): 6713-6726.

Rossoni AW, Price DC, Seger M, Lyska D, Lammers P, Bhattacharya D, Weber APM. 2019a. The genomes of polyextremophilic cyanidiales contain 1% horizontally transferred genes with diverse adaptive functions. *Elife* **8**, e45017.

Rossoni AW, Schonknecht G, Lee HJ, Rupp RL, Flachbart S, Mettler-Altmann T, Weber APM, Eisenhut M. 2019b. Cold Acclimation of the thermoacidophilic red alga *Galdieria sulphuraria*: Changes in gene expression and involvement of horizontally acquired genes. *Plant & Cell Physiology* **60**(3): 702-712.

Rossoni AW, Weber APM. 2019. Systems biology of cold adaptation in the polyextremophilic red alga *Galdieria sulphuraria*. *Front Microbiol* **10**, 927.

Schmidt RA, Wiebe MG, Eriksen NT. 2005. Heterotrophic high cell-density fed-batch cultures of the phycocyanin-producing red alga *Galdieria sulphuraria*. *Biotech Bioeng* **90**(1): 77-84.

Schonknecht G, Chen WH, Ternes CM, Barbier GG, Shrestha RP, Stanke M, Brautigam A, Baker BJ, Banfield JF, Garavito RM, et al. 2013. Gene transfer from bacteria and archaea facilitated evolution of an extremophilic eukaryote. *Science* **339**(6124): 1207-1210.

Schwaiger M, Rampler E, Hermann G, Miklos W, Berger W, Koellensperger G. 2017. Anion-exchange chromatography coupled to high-resolution Mass Spectrometry: A powerful tool for merging targeted and non targeted metabolomics. *Analytical Chemistry* **89**(14): 7667-7674.

Shim SH, Lee SK, Lee DW, Brilhaus D, Wu G, Ko S, Lee CH, Weber APM, Jeon JS. 2020. Loss of function of rice plastidic glycolate/glycerate translocator 1 impairs photorespiration and plant growth. *Front Plant Sci* **10**, 1726.

Sugawara H, Yamamoto H, Shihata N, Inoue T, Okada S, Miyake C, Yokota A, Kai Y. 1999. Crystal structure of carboxylase reaction-oriented ribulose 1,5-bisphosphate carboxylase oxygenase from a thermophilic red alga, *Galdieria partita*. *Journal of Biological Chemistry* **274**(22): 15655-15661.

Tcherkez G, Bligny R, Gout E, Mahe A, Hodges M, Cornic G. 2008. Respiratory metabolism of illuminated leaves depends on CO_2 and O_2 conditions. *Proc Nat Acad Sci USA* **105**(2): 797-802.

Villanova V, Fortunato AE, Singh D, Dal Bo D, Conte M, Obata T, Jouhet J, Fernie AR, Marechal E, Falciatore A, et al. 2017. Investigating mixotrophic metabolism in the model diatom *Phaeodactylum tricornutum*. *Philosophical Transactions of the Royal Society of London. Series B: Biological Sciences* **37**2: 20160404.

Wan MX, Liu P, Xia JL, Rosenberg JN, Oyler GA, Betenbaugh MJ, Nie ZY, Qiu GZ. 2011. The effect of mixotrophy on microalgal growth, lipid content, and expression levels of three pathway genes in *Chlorella sorokiniana*. *Applied Microbiol Biotech* **91**(3): 835-844.

Wieczorek S, Combes F, Borges H, Burger T. 2019. Protein-level statistical analysis of quantitative label-free proteomics data with ProStaR. *Methods in Molecular Biology* **1959**: 225-246.

835   **Wieczorek S, Combes F, Lazar C, Gianetto QG, Gatto L, Dorffer A, Hesse AM,**
836   **Coute Y, Ferro M, Bruley C, et al. 2017.** DAPAR & ProStaR: software to
837   perform statistical analyses in quantitative discovery proteomics.
838   *Bioinformatics* **33**(1): 135-136.
839   **Xu F, Hu HH, Cong W, Cai ZL, Ouyang F. 2004.** Growth characteristics and
840   eicosapentaenoic acid production by *Nannochloropsis sp.* in mixotrophic
841   conditions. *Biotech Lett* **26**(1): 51-53.
842   **Yoon H, Hackett JD, Ciniglia C, Pinto G, Bhattacharya D. 2004.** A molecular
843   timeline for the origin of photosynthetic eukaryotes. *Molecular Biology and*
844   *Evolution* **21**(5): 809-818.
845   **Yoon H, Hackett JD, Pinto G, Bhattacharya D. 2002.** The single, ancient origin
846   of chromist plastids. *Proc. Nat. Acad. Sci. USA* **99**: 15507–15512.
847   **Yoon HS, Ciniglia C, Wu M, Comeron JM, Pinto G, Pollio A, Bhattacharya D.**
848   **2006.** Establishment of endolithic populations of extremophilic Cyanidiales
849   (Rhodophyta). *BMC Evolutionary Biology* **6**(1): 78.

850
851
852
853   **Dataset S1:** Proteins involved in photosynthesis, central metabolism and
854   respiration were selected from the complete proteomic dataset (see
855   Supplementary Dataset S2) and used to build Fig. 3.
856
857   **Dataset S2:** Compared proteomic analysis between photoautotrophic, mixotrophic
858   and heterotrophic growth conditions.
859
860   **Dataset S3:** Compared metabolomic analysis between photoautotrophic,
861   mixotrophic and heterotrophic growth conditions.
862
863   **Figure S1**: Consequences of different substrates on *G. sulphuraria* growth in the
864   light.
865   **Figure S2:** *G. sulphuraria* growth in photoautotrophic, mixotrophic and
866   heterotrophic conditions driven by a polyol, an hexose and a disaccharide.
867   **Figure S3:** Experimental setup to expose cells to a constant photons/cell ratio.
868   **Figure S4:** *In situ* measurements of photosynthetic electron transfer rate (ETR) in
869   photoautotrophic (light) and mixotrophic (light + 25 mM D-sorbitol) cells.
870   **Figure S5:** Enhancement of cell growth by mixotrophy and sorbitol consumption
871   in *G. sulphuraria*.
872   **Figure S6:** Mixotrophy is restored in *G. sulphuraria* upon addition of a carbon
873   source.
874   **Figure S7:** Respiration and net photosynthesis were measured every day in the
875   three different growth conditions (photoautotrophy, mixotrophy and heterotrophy).
876   **Figure S8:** Biomass production as a function of transmitted light intensity and CO_2
877   concentration.
878   **Figure S9:** Immunodetection of RuBisCO in phototrophic and mixotrophic cultures
879   under ambient and enhanced CO_2 atmosphere.

880   **Figure S10:** Comparative analysis of phototrophic, mixotrophic and heterotrophic
881   performances in *G. sulphuraria* 074 G and SAG21.92 species with D-sorbitol and
882   D-glucose.
883   **Figure S11:** Respiration fuels photosynthesis in photoautotrophic and mixotrophic
884   *G. sulphuraria* cultures.
885   **Figure S12**: Transmission electron microscopy of *G. sulphuraria* SAG21.92 grown
886   5 days under photoautotrophic, mixotrophic and heterotrophic conditions.
887

888   **Methods S1:** Microalgae and media composition, growth, cell fresh weight and dry

889   weight estimates, Clark electrode oxygen and photophysiology measurements,

890   mass spectrometry-based proteomic analyses, metabolic analyses by IC-MS,

891   electron microscopy sample preparation and observation.

892

893

894

895
896 **Figure legends**

897

898 **Figure 1: Growth enhancement of *Galdieria sulphuraria* SAG21.92 by**
899 **reduced carbon sources is light dependent. a,** Growth curves. Data from 3
900 biological replicates ± S.D. Error bars are shown when larger than the symbol size.
901 *G. sulphuraria* was grown in flasks at ambient CO_2 in photoautotrophic (light only,
902 30 µmol photons m^{-2} s^{-1}, green), mixotrophic (30 µmol photons m^{-2} s^{-1} plus D-
903 sorbitol 25 mM, orange) and heterotrophic (absence of light, presence of D-sorbitol
904 25 mM, black). The initial cell concentration was 1.5 10^6 cells per mL. At day 5, the
905 mixotrophic culture was split in two parts, and light was switched off in one culture,
906 (grey). Growth was carried out at 42°C with shaking at 100 rpm, pH 2. **b,** Dry weight
907 estimated at day 9. Mixotrophic biomass (orange bars) exceeds the sum of
908 photoautotrophic (green bars) and heterotrophic (black bars) biomass, highlighting
909 the existence of a synergy under mixotrophic conditions. Data from 3 biological
910 replicates ± S.D. ** indicate that at the 0.01 level the means of the two populations
911 (mixotrophy on one side; heterotrophy + photoautotrophy on the other one) means
912 are statistically different (Anova test). The concentration of inorganic nitrogen was
913 20 mM, while that of inorganic phosphate was 5 mM.

914

915

916 **Figure 2: *In situ* measurements of photosynthetic electron transfer rate (ETR)**
917 **in photoautotrophic (light) and mixotrophic (light + 25 mM D-sorbitol)**
918 ***Galdieria sulphuraria* SAG21.92 cells and biomass production**. Cells were
919 inoculated at 3.5 10^6 cell per mL and grown in a photobioreactor in the light
920 (transmitted light 10 µmol photons m^{-2} s^{-1}) and air before D-sorbitol was added in
921 the absence (heterotrophy, black) and in the presence of light (mixotrophy,
922 orange). Light was increased every day to keep the transmitted light to a constant
923 value of 10 µmol photons m^{-2} s^{-1}. Growth was followed at 42°C and pH 2. **a, d, g**,
924 after five days of growth (*i.e.* 2 days after the addition of D-sorbitol), ETR was
925 measured directly on cultures within the photobioreactor, to avoid possible

926 temperature stress. Measurements were done in air, in the absence (**a, b**) and

927 presence (**d, e**) of respiratory inhibitors (SHAM 1 mM and myxothiazol (10 μM),

928 added 24 h before measurements), or in a CO_2-enriched (0.5%) atmosphere (**g,**

929 **h**). **a**, **b**, **g** photosynthetic electron transfer: data from 3 biological replicates ± S.D.

930 **b**, **e**, **h**, Biomass production in photoautotrophic (green, data from 12 biological

931 replicates ± S.D.), heterotrophic (black, data from 8 biological replicates ± S.D.)

932 and mixotrophic (orange, data from 8 biological replicates ± S.D.) conditions,

933 respectively. Cells were collected after 7 days of growth (i.e. 4 days after addition

934 of D-sorbitol). **c, f, i,** Sketches representing possible CO_2 sources for

935 photosynthesis in the three examined conditions. ** indicate that at the 0.01 level

936 the means of the two populations (mixotrophy on one side;

937 heterotrophy+photoautotrophy on the other one) means are statistically different

938 (Anova test).

939

940 **Figure 3: Synthesis of proteomic changes between phototrophic,**

941 **mixotrophic and heterotrophic growth conditions of *Galdieria sulphuraria***

942 **SAG21.92**. Plastid is indicated in green, cytosol in white, mitochondrion in orange

943 and peroxisome in grey. Proteins are identified by their SwissProt accessions;

944 boxes on top of protein names represent fold-changes (protein average

945 abundance in one condition was compared with the average abundance of the

946 other two conditions - left photoautotrophy, middle mixotrophy, right heterotrophy).

947 Proteins displaying statistically significant changes (see methods) are highlighted

948 in yellow. They include proteins involved in carbon concentrating mechanism

949 (Pyruvate phosphate dikinase -M2XY57, carbonic anhydrase-M2XTP2, PEP

950 carboxylase-M2XIX2), which are much more abundant in photoautotrophic

951 conditions than in mixotrophic or heterotrophic conditions. Enzymes involved in

952 photorespiration-dashed arrows-(Phosphoglycolate phosphatase-M2XAQ1,

953 Glycolate oxidase-M2WRR8, Serine-glyoxylate aminotransferase-M2Y9J6,

954 Glycine decarboxylase P proteins-M2X9U4, Glycine/serine

955 hydroxymethyltransferase-M2XX08, Hydroxypyruvate reductase-M2XII5,

956 Glycerate kinase-M2XRC5) follow the same pattern as CCM enzymes.

957   Conversely, pyruvate kinases (especially M2WVY6) are strongly repressed under

958   phototrophic condition, possibly to maintain a high PEP-oxaloacetate (OAA) pool

959   for efficient fluxes in the carbon concentration cycle. Enzymes involved in

960   photosynthesis are reduced under mixotrophic condition compared to

961   photoautotrophic condition and strongly reduced under heterotrophic conditions.

962   Mitochondrial respiratory proteins involved in the Krebs cycle or in ATP production

963   are virtually not affected with the exception of fumarase and malic enzyme strongly

964   reduced under phototrophic condition. Only representative proteins of the different

965   complexes (*e.g.* photosynthesis, respiration) are represented. A more complete list

966   of proteins can be found in Dataset S1. The complete set of proteomic data is

967   available in Dataset S2.

968

969   **Figure 4: Metabolic changes between phototrophic, mixotrophic and**

970   **heterotrophic growth conditions of *Galdieria sulphuraria* SAG21.92.** Non-

971   phosphorylated metabolites were analyzed by GC-MS, phosphorylated

972   metabolites were analyzed using IC-MS. Quantification of metabolites is provided

973   in Dataset S3. Green bars: photoautotrophy; orange bars: mixotrophy; black bars:

974   heterotrophy. **a**, Changes of metabolites involved in photorespiration. 2P-glycolate

975   as a photorespiration-specific metabolite is boxed in red. Glycolate, glycine, serine

976   and glycerate are transported between cellular compartments as indicated by

977   dashed arrows. PGLP: phosphoglycolate phosphatase; GOX: glycolate oxidase;

978   GGAT: glutamate:glyoxylate aminotransferase; GDC: glycine decarboxylase

979   complex; SHMT: serine hydroxymethyltransferase; SGAT: serine:glyoxylate

980   aminotransferase; HPR: hydroxypyruvate reductase; GLYK: glycerate kinase. **b**,

981   Metabolites involved in a putative C4-type CCM. CA: Carbonic anhydrase; PPC:

982   phosphoenolpyruvate carboxylase; PEPCK: phosphoenolpyruvate carboxykinase;

983   PPDK: pyruvate phosphate dikinase; PEP: phosphoenolpyruvate. **c**, Metabolic

984   changes of intermediates of upper glycolytic pathways (EMP, ED, PPP) and

985   purine/ pyrimidine metabolism. The pentose-5P (ribulose-5P, xylulose-5P, ribose-

986   5P, marked with an asterisk) could not be distinguished and are plotted in a single

987   boxed graph. SDH: sorbitol dehydrogenase; FRK: fructokinase; GPI: glucose-6P

988 isomerase; G6PD: glucose-6P dehydrogenase; GND: 6-phosphogluconate
989 dehydrogenase; EBB: phosphogluconate dehydratase; EDA: KDPG aldolase;
990 PFK: 6-phosphofructokinase; FBPase: fructose-1,6P bisphosphatase; FBA:
991 fructose bisphosphate aldolase; TIM: triosephosphate isomerase; RPE: ribulose-
992 5P epimerase; RPI: ribulose-5P isomerase; TKT: transketolase; TAL:
993 transaldolase. The full list of metabolite changes can be found in Dataset S3. Y
994 axes in the graphs correspond to normalized peak areas and error bars represent
995 the standard deviation of biological quadruplicates.

996

997

998 **Figure 5: Incorporation of carbon derived from ^{13}C-labelled glucose into**
999 **intermediates of the Calvin-Benson-Bassham (a) and tricarboxylic acid (b)**
1000 **cycles during mixotrophic cultivation of *Galdieria sulphuraria* SAG21.92 in**
1001 **two different CO_2 concentrations.** Incorporation rates are displayed as average
1002 number of labelled carbon atoms in each molecule (average exchange). Error bars
1003 represent the standard deviation of biological quadruplicates. Light orange: cells
1004 grown in ambient air (0.02% CO_2). Dark orange cells grown in air supplied with 2%
1005 CO_2.
1006 RuBP: Ribulose 1,5-bisphosphate; 3-PGA: 3-phosphoglycerate; 2-PG: 2-
1007 phosphoglycolate; BPG: 1,3-bisphosphoglycerate; DHAP: Dihydroxyacetone
1008 phosphate; GAP: glyceraldehyde 3-phosphate; FBP: Fructose 1,6-bisphosphate;
1009 F6P: Fructose 6-phosphate; E4P: Erythrose 4-phosphate; Xu5P: Xylulose 5-
1010 phosphate; SBP: Seduheptulose 1,7-bisphosphate; S7P: Seduheptulose 7-
1011 phosphate; R5P: Ribose 5-phosphate; Ru5P: Ribulose 5-phosphate.

1012

1013
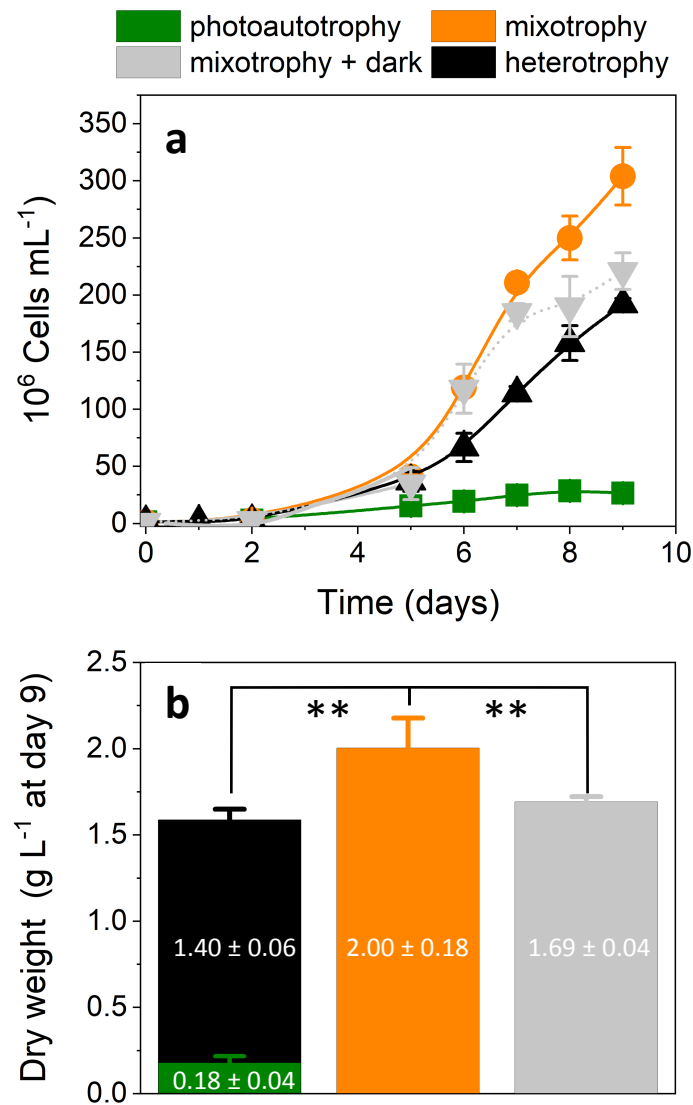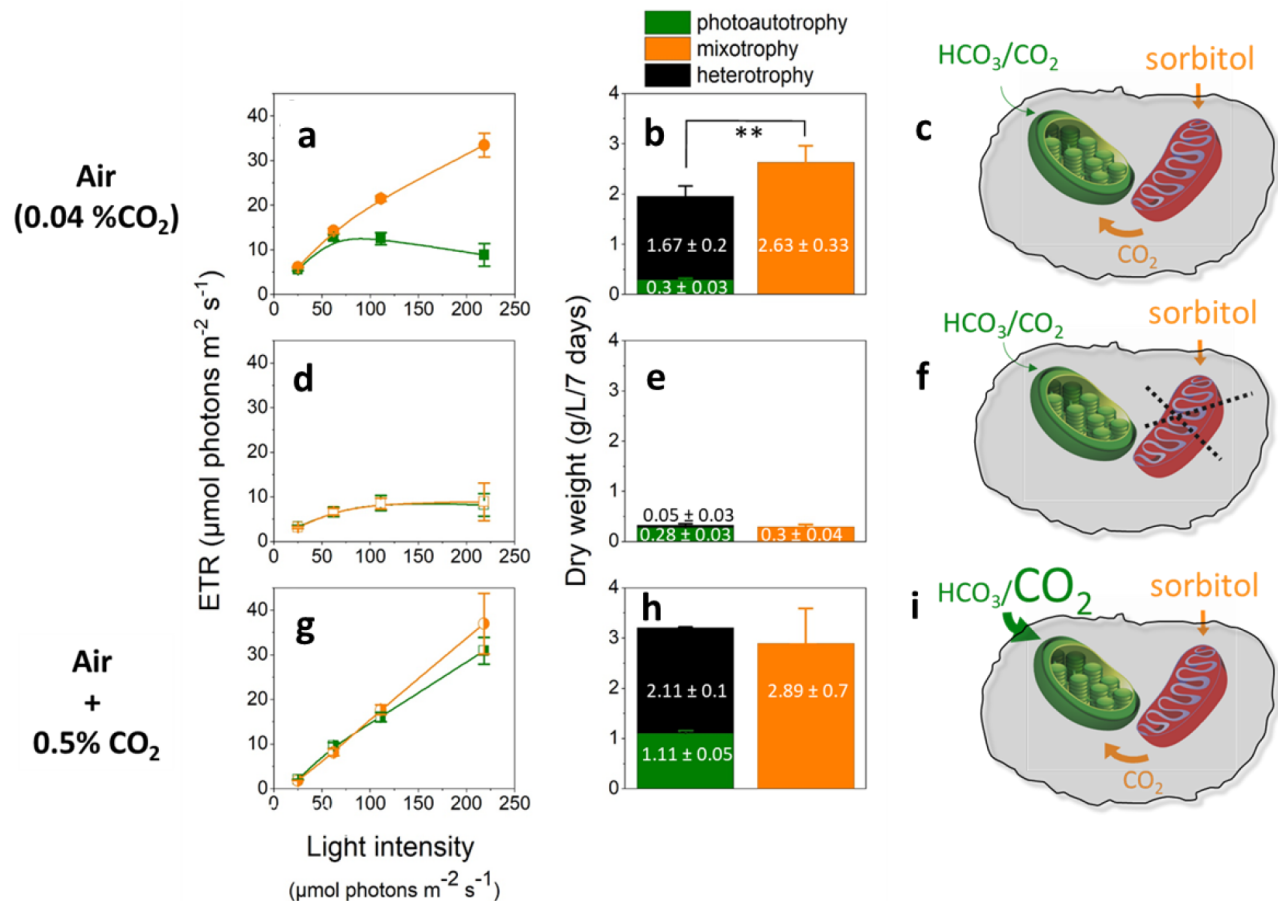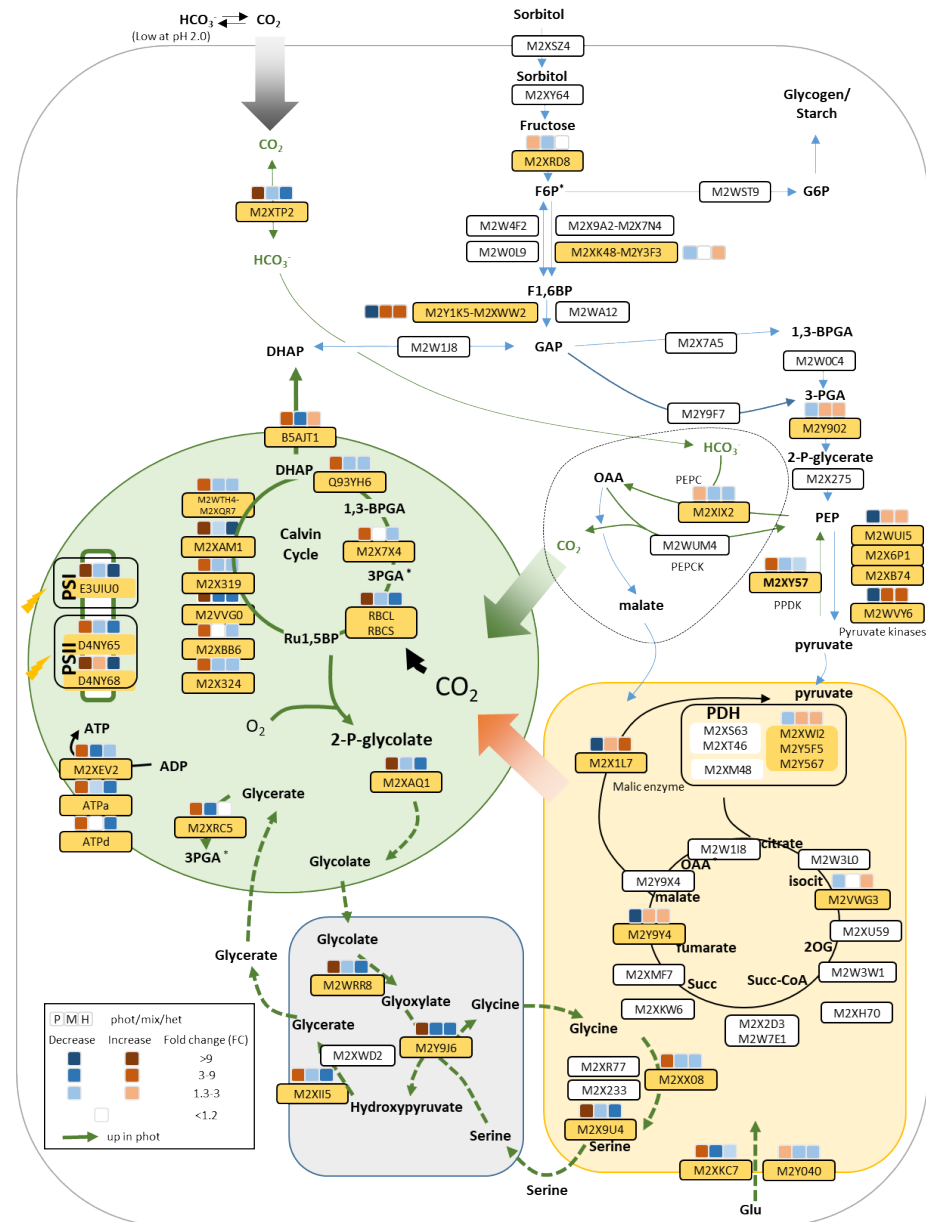
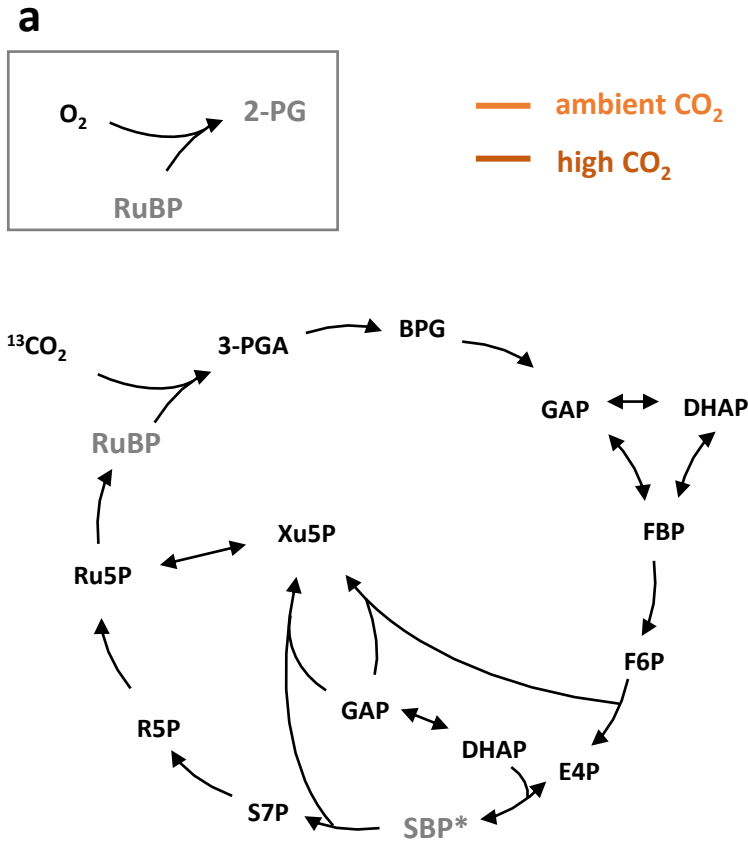Figure 1

Figure 2

Figure 3
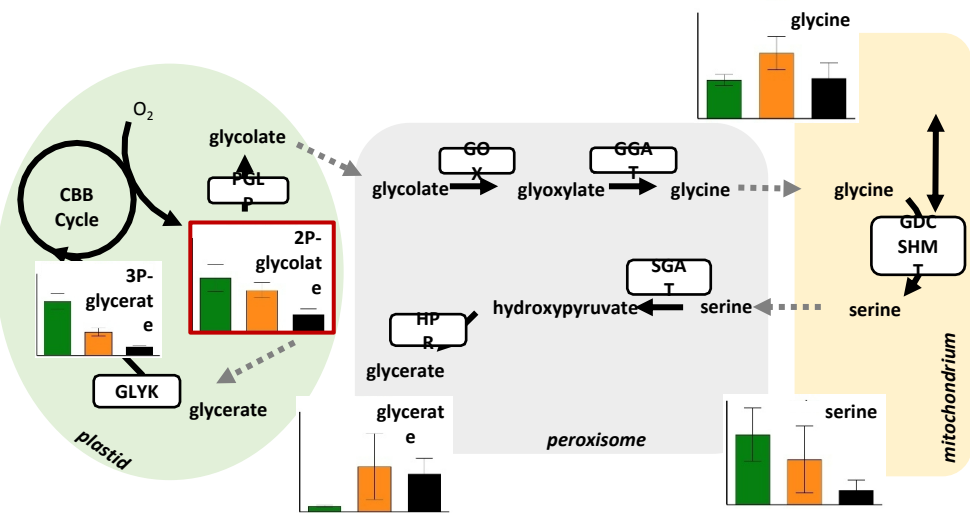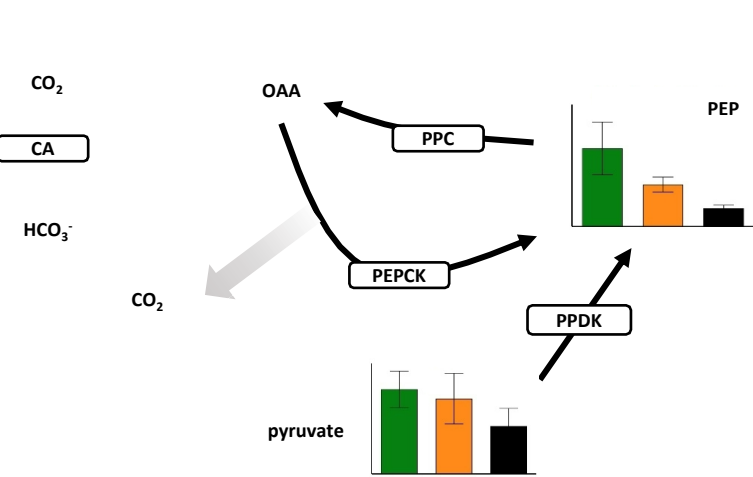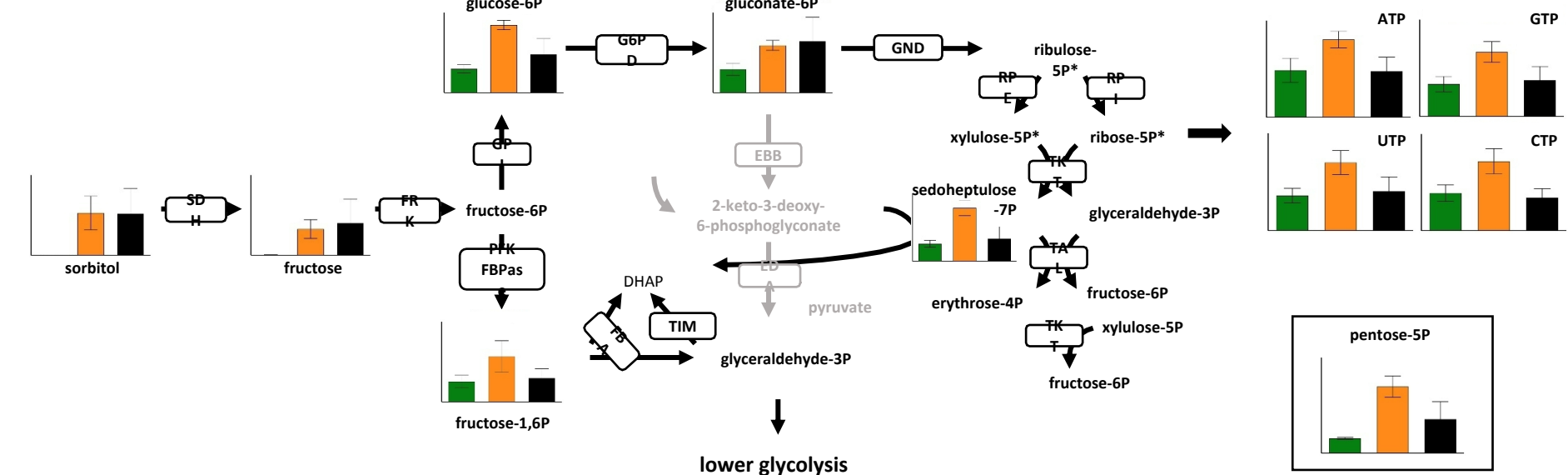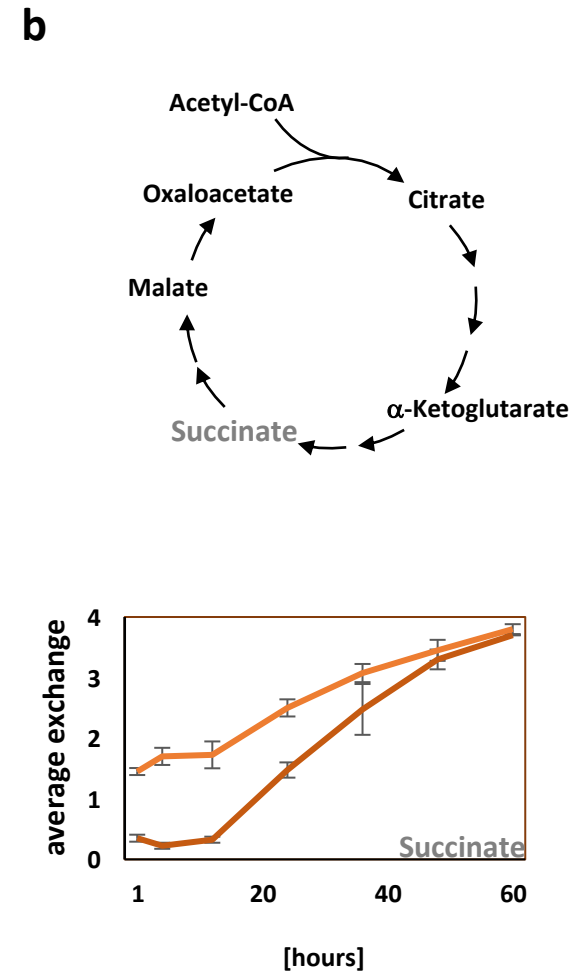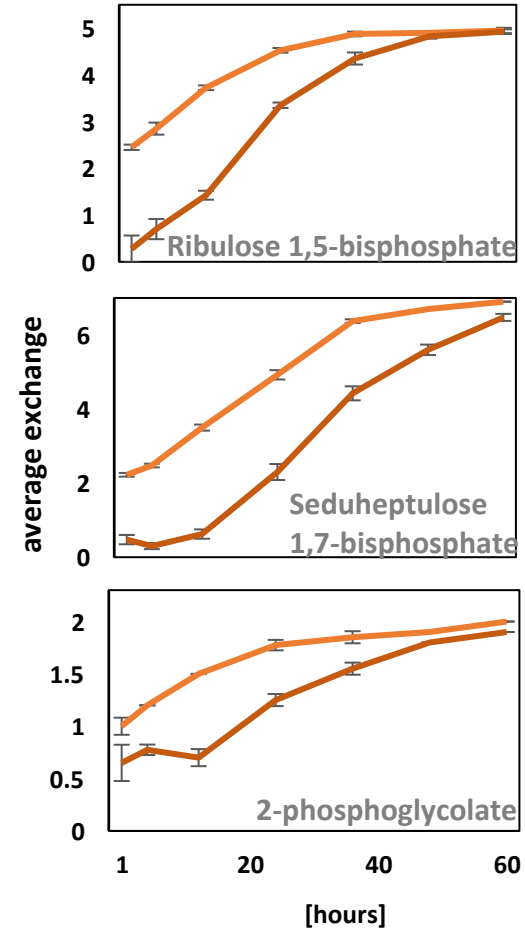
Figure 4

Figure 5

Supporting Information for

MIXOTROPHIC GROWTH OF THE EXTREMOPHILE *GALDIERIA SULPHURARIA* REVEALS THE FLEXIBILITY OF ITS CARBON ASSIMILATION METABOLISM

Gilles Curien[1]*, Dagmar Lyska[2], Erika Guglielmino[1], Phillip Westhoff[2], Janina Janetzko[2], Marianne Tardif[3], Clément Hallopeau[1], Sabine Brugière[3], Davide Dal Bo[1], Johan Decelle[1], Benoit Gallet[4], Denis Falconet[1], Michele Carone[5], Claire Remacle[5], Myriam Ferro[3], Andreas P.M. Weber[2], Giovanni Finazzi[1]

[1]Laboratoire de Physiologie Cellulaire et Végétale. Univ. Grenoble Alpes, CNRS, CEA, INRA, 38054 Grenoble Cedex 9, France

[2]Institute of Plant Biochemistry, Cluster of Excellence on Plant Sciences (CEPLAS), Heinrich Heine University, Düsseldorf, Germany

[3]EdyP Laboratoire Biologie à Grande Echelle. Univ. Grenoble Alpes, CEA, Inserm, BGE U1038, 38054 Grenoble Cedex 9, France

[4]Institut de Biologie Structurale, Univ. Grenoble Alpes, CNRS, CEA, 71 Avenue des Martyrs, 38044 Grenoble, France

[5]Genetics and Physiology of microalgae, InBios/Phytosystems Research Unit, University of Liege, Belgium

* Corresponding author: Gilles Curien. phone: +33 4 38782509, email**:** gilles.curien@cea.fr

article acceptance date: 18 March 2021.

This file includes:

    Methods S1
    Figures S1 to S12
    Legends for Datasets S1 to S3

Other supplementary materials for this manuscript include the following:

    Datasets S1 to S3

Methods S1

Microalgae and media composition

Galdieria sulphuraria SAG21.92 and 074G were obtained from the Culture Collection of Algae at Göttingen University (SAG) and was grown in sterile 2xGS modified Allen medium, pH 2.0, containing 20 mM of $NaNO_3$, and 5 mM of inorganic phosphate (K_2HPO_4 and KH_2PO_4 in a 2/1 ratio, (Allen, 1959)) at 42°C. The medium and flasks were sterilized in an autoclave for 20 min at 121 °C in order to prevent any contamination. For the experiments with different organic carbon sources, the 2xGS modified Allen media was supplemented by adding filter-sterilized concentrated organic substrate solutions as indicated in the text. The concentration of organic substrates was selected on the basis of data reported in literature (Oesterhelt *et al.*, 2007). *G. sulphuraria* was grown either in 250 mL flasks (50 mL culture volume) in an incubator (Infors, Switzerland, continuous light, 30 µmol photons m^{-2} s^{-1}, 42°C, 100 rpm) or in a multicultivator (Photon System Instruments, Czech Republic). For growth in the multicultivator, cells were provided with air or CO_2-enriched air (see below) bubbled into the solution ensuring both aeration and mixing. Culture volume was 80 mL. Incident light intensity was adjusted daily to maintain constant transmitted light thus offering a constant light intensity to the cells (see Results and below). The fraction of CO_2 in the feed air was regulated by a flow metering system (Photon System Instruments, Czech Republic). The total gas flow was 0.4 L/min for each culture.

Growth

Cultures used to inoculate flasks or multicultivator tubes were grown photoautotrophically in the air in flasks placed in the incubator. Adequate volumes of cultures at a density of 7×10^7 cells per mL were centrifuged and resuspended in a fresh medium to obtain an initial cell concentration of 1.5×10^6 cells per mL (in flasks) or 3.5×10^6 cells per mL (multicultivator). For organic substrates screening in flasks under mixotrophic conditions (see Fig. S1 & S2), substrate was added at a concentration of 150 mM carbon atom (*e.g.* 12.5 mM saccharose). For growth in the multicultivator cells were adapted for 3 days with an incident light of 60 µmol

2

photons m^{-2} s^{-1} (transmitted light ~ 10 µmol photons. $m^2.s^{-1}$), before addition of organic carbon (150 mM C) for the mixotrophic and heterotrophic conditions. For the heterotrophic condition, light was switched-off and tubes were covered with aluminum foil to keep them in the dark. For experiments with the multicultivator, the incident light intensity was adjusted daily to maintain constant transmitted light though the culture (see Results). This 'luminostat' regime should ensure maximal absorption of light without allowing a dark zone to develop inside the multicultivator (Cuaresma *et al.*, 2011) (see Supplementary Fig. S3). For most conditions, a transmitted light of 10 µmol photons m^{-2} s^{-1} was used. Tests were carried out in the range from 5 to 30 µmol photons m^{-2} s^{-1} (see Supplementary Fig. S8). Experiments were either carried out in air or in air enriched with CO_2 (0.5 to 4%, see Supplementary Fig. S8). Sorbitol consumption was measured using the D Sorbitol/Xylitol assay kit (Megazyme).

To monitor algal growth, samples were taken daily and growth was estimated using a LUNA™ cell counter (Logos Biosystems, Inc. USA).

Cell fresh weight and dry weight estimates

Cells were collected by centrifugation in 50 mL tubes, cell pellet was resuspended in a small volume of water and centrifuged in pre-weighted eppendorf tubes and pellet was weighted. For dry weight determination fresh cells pellets were exposed for three days at 60°C, weighted and expressed as g L^{-1}.

Clark electrode oxygen measurements

Net oxygen exchanges in solution were measured with a Clark-type electrode (Hansatech Instruments, UK) at 42°C. The electrode equilibrated for 12 h in distilled water was calibrated at 42°C in the air (100% of O_2) and by bubbling argon (0% of O_2). For oxygen exchanges measurements, an aliquot of the cell culture was collected immediately before the measurement (30 10^6 cells) and centrifuged at 42°C. The pellet was resuspended in 1 mL 2 x GS medium, pH 2.0, 42°C and introduced in the measure chamber thermostated at 42°C. The electrode was closed and measurement was first carried out in the dark for 10 minutes before light was switched on (320 µmol photons m^{-2} s^{-1}). Respiration and gross

photosynthesis were quantified by measuring the slope of oxygen changes in the dark and under light exposure. Net photosynthesis was calculated assuming O_2 consumption by the mitochondrion in the light is identical to that in the dark (Net photosynthesis = $v_{O2light} + |v_{O2dark}|$).

Photophysiology measurements

Photosynthetic parameters were derived from quantification of chlorophyll fluorescence emission by cultures within the multicultivator. To this aim, we employed a custom-made fluorescence imaging system based on a previously published setup (Johnson *et al.*, 2009). The system was modified by replacing the green LEDs providing actinic light with orange LEDs (emission peak 630 nm, Full Width at Half Maximum: 40 nm), and the acquisition setup with a GigE µeye camera (IDS, Germany). Measuring light was provided by a LED peaking at 590 nm, to maximize excitation of the phycobiliprotein complexes of Galdieria. The photosynthetic electron transfer rate, ETR_{PSII}, was calculated as the product of the light intensity times the photochemical yield in the light (Fm'-Fs)/Fm' x PFD, where Fm' and Fs are the fluorescence intensities measured after exposure to a saturating pulse and in steady state, respectively, in light-acclimated cells and PFD (Photosynthetic Flux Density) is the incident light intensity, measured in µmol photons m-2 s-1.(see (Maxwell & Johnson, 2000) for more details). Cells were allowed to reach steady state fluorescence emissions at every light (5-10 minutes of light exposure depending on the intensity) before increasing the photon flux.

Mass spectrometry-based proteomic analyses

<u>Experimental design</u>

Galdieria sulphuraria SAG21.92 was cultivated under the three conditions (photoautotrophy, mixotrophy and heterotrophy) in parallel in the same cultivator (2-3 tubes per condition). Three multicultivator experiments were carried out one week apart and constituted the biological replicates. Only one tube per condition and per cultivator was chosen having the closest ODs within the same condition.

Cell breakage was performed on 10^9 cells with a Precellys homogenizer (Bertin, France).

Protein digestion

Each protein sample (40 µg) was stacked by a 1 cm-migration on the top of a NuPAGE 4–12% gel, (Invitrogen) before Coomassie blue staining (R250, Bio-Rad). Gel bands of concentrated proteins were manually excised and cut into pieces before being washed by 6 successive incubations of 15 min in 25 mM NH_4HCO_3 containing 50% (v/v) acetonitrile. Gel pieces were then dehydrated in 100% acetonitrile and incubated at 53 °C with 10 mM DTT in 25 mM NH_4HCO_3 for 45 min and in the dark with 55 mM iodoacetamide in 25 mM NH_4HCO_3 for 35 min. Alkylation was stopped by adding 10 mM DTT in 25 mM NH_4HCO_3 and mixing for 10 min. Gel pieces were then washed again by incubation in 25 mM NH_4HCO_3 before dehydration with 100% acetonitrile. Modified trypsin (Promega, sequencing grade) in 25 mM NH_4HCO_3 was added to the dehydrated gel pieces for an overnight incubation at 37 °C. Peptides were then extracted from gel pieces in three 15-min sequential extraction steps in 30 µl of 50% acetonitrile, 30 µl of 5% formic acid and finally 30 µl of 100% acetonitrile. The pooled supernatants were then vacuum-dried.

MS/MS analysis

The dried extracted peptides were resuspended in acetonitrile 5%, trifluoroacetic acid 0.1% and analyzed via online nano-LC-MS/MS (nano-liquid chromatography-tandem mass spectrometry; Ultimate 3000 RSLCnano and Q-Ex HF, Thermo Fischer Scientific, Thermo Scientific, Waltham, MA, USA). Peptide mixtures were desalted on line using a reverse phase precolumn (PepMap C18 Thermo Fisher Scientific) and resolved on a C18 column (ReproSil-Pur 120 C18-AQ 1.9 µm column, Dr. Maisch GmbH). The nanoLC method consisted in a 200-min gradient at a flow rate of 300 nL·min−1 ranging from 5.1% to 72.2% acetonitrile in 0.08% formic acid in 182 min. This gradient was operated as multi-steps optimized by GOAT software (V1.0.1) for Galdieria whole cell extracts. MS (mass spectrometry) and MS/MS data were acquired using the Xcalibur software (Thermo Fisher

Scientific). The spray voltage was set at 2 kV and the heated capillary was adjusted to 270 °C. Survey full-scan MS spectra (m/z = 400–1600) were obtained in the Orbitrap with a resolution of 60,000 after accumulation of 10^6 ions (maximum filling time: 200 ms). The 20 most intense ions from the preview survey scan delivered by the Orbitrap were fragmented via collision-induced dissociation in the LTQ after accumulation of 1e5 ions (maximum filling time: 50 ms).

Database searches and quantification

Data were processed automatically using the Mascot Distiller software (version 2.7.1.0, Matrix Science). Peptides and proteins were identified using Mascot (version 2.6.0) through concomitant searches against Uniprot (*Galdieria sulphuraria* taxonomy, July 2019 version), classical contaminants database (homemade) and their corresponding reversed databases. Trypsin/P was chosen as the enzyme and three missed cleavages were allowed. Precursor and fragment mass error tolerance were set, respectively, to 10 ppm and 25 mmu. Peptide modifications allowed during the search were: carbamidomethylation (fixed), acetyl (protein N-terminal, variable) and methionine oxidation (variable). The Proline software ((Bouyssie *et al.*, 2020), http://proline.profiproteomics.fr) was used to filter the merged results: conservation of rank 1 peptide-spectrum match (PSM) with a minimal length of 7 and a minimal score of 25. PSM score filtering is then optimized to reach a False Discovery Rate (FDR) of PSM identification below 1% by employing the target decoy approach. A minimum of one specific peptide per identified protein group was set. Proline was then used to perform MS1-based label free quantification of the peptides and protein groups. The "Cross-assignment" option was activated and allowed within replicates of the same condition only. Intensity values were extracted from specific peptides and used to infer protein abundances from the different samples. An ultimate filter was applied to discard non-relevant or doubtful identifications. This concerns proteins identified in the reverse and contaminant databases, proteins identified with only one peptide with a Mascot score inferior to 40 and few unquantified proteins. Proteins identified in the reverse and contaminant databases (i.e. trypsin or keratin), and proteins identified with only 1 peptide with a score <40 were further discarded from the list.

Statistical treatment

The remaining list was considered for bioanalysis. Since there were many missing proteins in the photoautotrophy condition compared to the other two conditions, the list was divided into two sets. One set on which no statistical treatment was applied was constituted of proteins entirely missing in one condition (having no abundance values in all 3 replicates). The other set (proteins having at least 1 abundance value in all three conditions) was used for differential analysis using ProStaR (Wieczorek *et al.*, 2017; Wieczorek *et al.*, 2019). For this, the intensity values were log2 transformed and normalized by Variance Stabilizing Normalization (VSN) algorithm (Huber *et al.*, 2002) with the « overall » option. The missing abundances were imputated according to the Structured Least Square Adaptative (SLSA) method. The Limma test was applied for comparison of one condition versus the other two combined. Due to huge differences in the matrix – proteins identified and intensities – in photoautotrophy compared to mixotrophy or heterotrophy, the strategy consisting of comparing one condition to the average of the other two (option "One_vs_All" in ProStaR) gave better discriminating results than comparisons of one condition to another one condition ("One_vs_One" option in ProStaR). Differentially recovered proteins were sorted out using a log2 fold-change (FC) cut-off of 1 and a p-value threshold (on the remaining proteins) that guarantees a Benjamini–Hochberg FDR of approximately 0.01%. The variations in abundance between the three cultivation conditions are important which made it difficult to objectively determine the latter threshold. We deliberately chose a very low FDR threshold to select a protein set of reasonable size in each comparison.

Metabolic analyses by IC-MS

The dried sample was reconstituted in 100 µL deionized water and 5 µL were injected via a Dionex AS-AP autosampler in push partial mode with a 10 µL loop. The temperature of the autosampler was set to 4 °C to maintain sample stability. Anion exchange chromatography was conducted on a Dionex IonPac AS11-HC column (2 mm × 250 mm, 4 µm particle size, Thermo Scientific) equipped with a Dionex IonPac AG11-HC guard column (2 mm × 50 mm, 4 µm, Thermo Scientific)

at 30 °C. The mobile phase was established using an eluent generator with a potassium hydroxide cartridge to produce a potassium hydroxide gradient. The column flow rate was set to 380 µL min^{-1} with a starting KOH concentration of 10 mM. The concentration was held for 3 min, then increased to 50% within 9 min followed by a steeper increase to 100% within 7 min. After 2 min of plateau the concentration dropped immediately back to 10 % for 8 min of equilibration. To prevent the high amounts of salt from entering the ESI source a Dionex ADRS 600, 2 mm suppressor was used in dynamic mode at a temperature of 15 °C. Spray stability was achieved with a make up consisting of methanol with 10 mM acetic acid delivered with 150 µL min^{-1} by an AXP Pump. The electro spray was achieved in the ESI source using the following parameters: sheath gas 30, auxiliary gas 15, sweep gas 0, spray voltage - 2.8 kV, capillary temperature 300 °C, S-Lens RF level 45, and auxiliary gas heater 380 °C. For the untargeted approach the mass spectrometer operated in a combination of full mass scan and a data-dependent Top5 MS2 (ddMS2) experiment. The full scan (60-800 m/z) was conducted with a resolution of 140.000 and an automatic gain control (AGC) target of 10^6 ions with a maximum injection time (IT) of 500 ms. The Top5 ddMS2 experiment was carried out with a resolution of 17.500 and an AGC target of 10^5 and a maximum IT of 50 ms. The stepped collision energy was used with the steps (15,25,35) to create an average of NCE 25.

Untargeted data analysis was conducted using Compound Discoverer (version 3.1, Thermo Scientific) using the "untargeted Metabolomics workflow". In this workflow automatic retention time alignment is performed in a window of 2 min within 5 ppm mass accuracy as well as unknown compound detection, and compound grouping across all samples. Elemental compositions are predicted based on accurate mass and chemical background is substracted by using blank extraction samples. Levels of peak annotation are indicated in the supplementary Dataset S3. Lowest level of annotation is based on accurate mass (3 ppm mass accuracy) on MS^1 level and allows to evaluate potential sum compositions and comparisons with databases such as Chemspider (http://www.chemspider.com) with ranking by the mzLogic algorithm. The next level of identification is via MS^2

level by comparing MS^2 fragment spectra using mzCloud (ddMS2) (match factor 50) and MS^1 level ChemSpider (by formula or exact mass). Highest identification level via an in-house MS^2 spectral library and retention time was established using mzVault. QC-based batch normalization was performed with QC sample injection every 5 samples during the sequence. Differential analysis, determination of p-values, adjusted p-values, ratios, fold change, were also calculated using Compound Discoverer.

Labelling experiments with ^{13}C-glucose

Cells were cultivated in 250 mL Erlenmeyer flasks (50 mL culture volume) for four days under continuous light at 60 µmol m-2 s-1, 40 °C and ambient air (0.04% CO_2). U-$^{13}C_6$-glucose (Cambridge Isotope Laboratories Inc, Tewksbury, Massachusetts) was added at day 4 in a final concentration of 25 mM and the irradiance was increased to 100 µmol m-2 s-1 either under ambient or elevated (2%) CO_2 conditions.

1-2.5 x10^8 cells were harvested 1, 4, 12, 24, 36, 48 and 60 hours after glucose addition as described above. Metabolites were extracted and measured by IC-MS as described above.

Data analysis was conducted with Compound Discoverer (version 3.1, Thermo Scientific) and the standard workflow for stable isotope labelling from Compound Discoverer was chosen. The default settings, which are 5 ppm mass tolerance, 30 % intensity tolerance and 0.1 % intensity threshold for isotope pattern matching were used and the maximum exchange rate was set to 95%.

Electron microscopy sample preparation and observation

Cells were pelleted (1000g, 5 min, 4°C) and fixed in reduced osmium tetroxide. To this end, cell pellets were resuspended in 0.1 M phosphate buffer (pH 7.4) and 2.5% glutaraldehyde and incubated overnight at 4°C. Cells were then pelleted and washed five times in 0.1 M phosphate buffer. Cells were fixed by a 1h incubation on ice in 500 µL 0.1 M phosphate buffer containing 1% osmium and 1.5% ferricyanide potassium red before they were pelleted and washed five times with

0.1 M phosphate buffer. Pellets were resuspended in 0.1 M phosphate buffer containing 0.1% tannic acid and incubated for 30 min in the dark at room temperature. Again, cells were pelleted and washed five times with 0.1 M phosphate buffer. The samples were dehydrated in ascending sequences of ethanol and infiltrated with ethanol/Epon resin mixture. Finally, the cells were embedded in Epon. Ultrathin sections (70 nm) were prepared with a diamond knife on a PowerTome ultramicrotome (RMC products) and collected on nickel grids. Ultrathin sections were examined on a Philips CM120 transmission electron microscope operating at 80 kV.
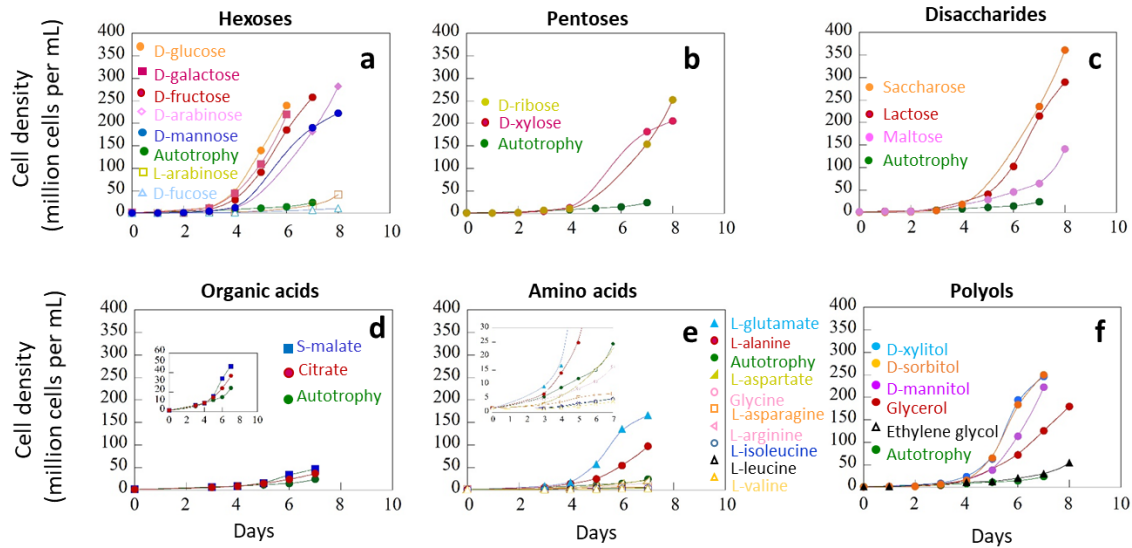
Figure S1: Consequences of different substrates on *G. sulphuraria* SAG21.92 growth in the light. Growth was measured in flasks at ambient CO_2 in the presence of 25 mM reduced carbon source added from the beginning of the culture (day 0). Cultures were inoculated at a cell density of $1.5 \cdot 10^6$ photoautotrophic cells mL^{-1}. Growth of photoautotrophic cells is indicated in green, for comparison. Light intensity was 30 µmol photons m^{-2} s^{-1}. Experiments were carried out at 42°C with shaking at 100 rpm, pH 2. **a**, hexoses, **b**, pentoses, **c**, disaccharides, **d**, organic acids, **e**, amino acids, **f**, polyols. Inserts in panel **d** and **e** are zooms on the data.
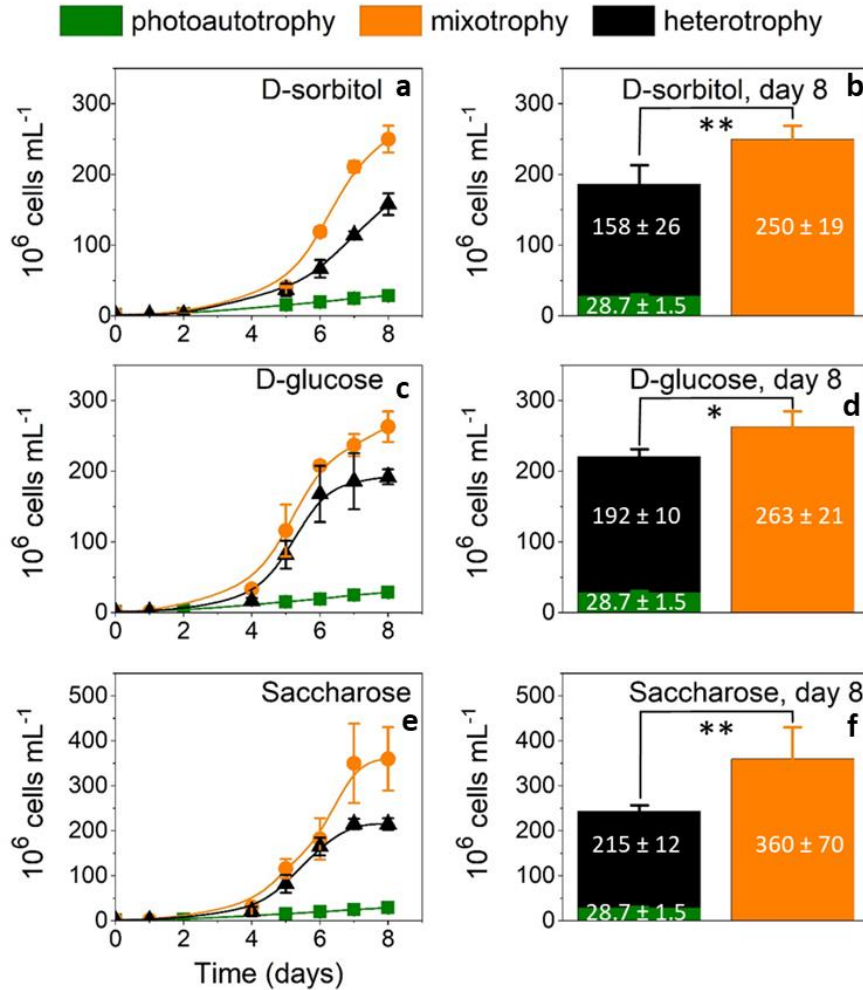
Figure S2: *G. sulphuraria* **SAG21.92 growth in photoautotrophic, mixotrophic and heterotrophic conditions driven by a polyol, an hexose and a disaccharide**. Cells were grown in flasks, in photoautotrophic (light only, 30 µmol photons m^{-2} s^{-1}, green), mixotrophic (30 µmol photons. $m^{-2}.s^{-1}$ plus a source of reduced carbon, orange) and heterotrophic (absence of light, presence of a source of reduced carbon, black) conditions at ambient CO_2, 42°C and pH 2. **a,b**: D-sorbitol 25 mM; **c,d**: D-glucose 25 mM; **e,f**: saccharose 12.5 mM. **b-d-f**: Mixotrophic growth (orange bars) exceeds the sum of photoautotrophic (green bars) and heterotrophic (black bars) growth, highlighting the existence of a synergy under mixotrophic conditions. Cultures were started from photoautotrophic cells, which were diluted at 1.5 10^6 cells mL^{-1} for each condition. Experiments were carried out at 42°C with shaking at 100 rpm. **b, d, f**, Final cell concentration (day 8) in photoautotrophic, heterotrophic and mixotrophic conditions. Data from 3 biological replicates ± S.D. * indicate that at the 0.05 level the means of the two populations (mixotrophy on one side, heterotrophy+photoautotrophy on the other one) means are s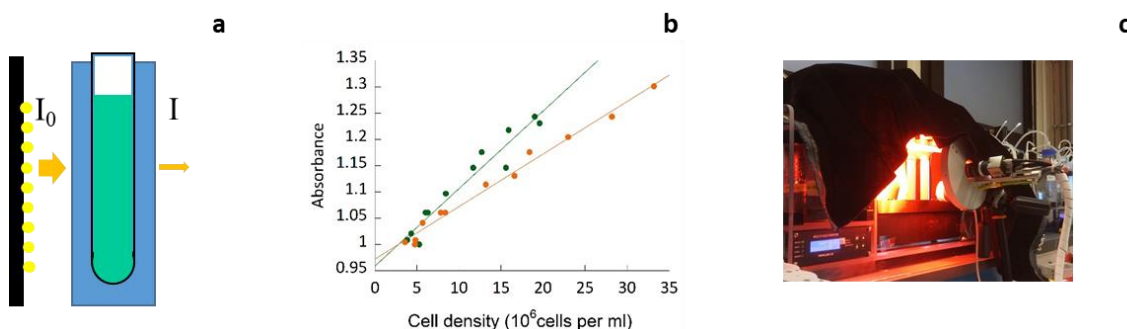tatistically different (Anova test). ** indicate that at the 0.01 level the means of the two populations (mixotrophy on one side, heterotrophy+photoautotrophy on the other one) means are statistically different (Anova test).

Figure S3: Experimental setup to expose cells to a constant photons/cell ratio. **a**, Schematic side view of the photobioreactor with the LED panel (yellow spots), water bath (blue) and culture tube (green). I_0 and I represent the incident light (settings on the device) and the light transmitted through the device, respectively. I_0 was progressively increased during cell growth, to keep a linear relation between cell density and absorption. **b**, Relation between absorbance and cell number under mixotrophic and photoautotrophic conditions for $I = 10$ µmol photons m^{-2} s^{-1}. The slopes differ for mixotrophic (orange) and photoautotrophic (dark green) cells possibly because the photosynthetic apparatus is down-regulated in the presence of organic carbon. The lower amount of photosynthetic complexes reduces light absorption for the same amount of cell. **c**, Custom-made setup to evaluate photosynthetic performances of *G. sulphuraria* cells within the photobioreactor. The system is equipped with orange LEDs ($\lambda = 590$ nm), to enhance absorption by the phycobiliprotein complexes of *G. sulphuraria*, and a near infrared camera to measure fluorescence emitted by the algae inside the photobioreactor (PBR tubes).
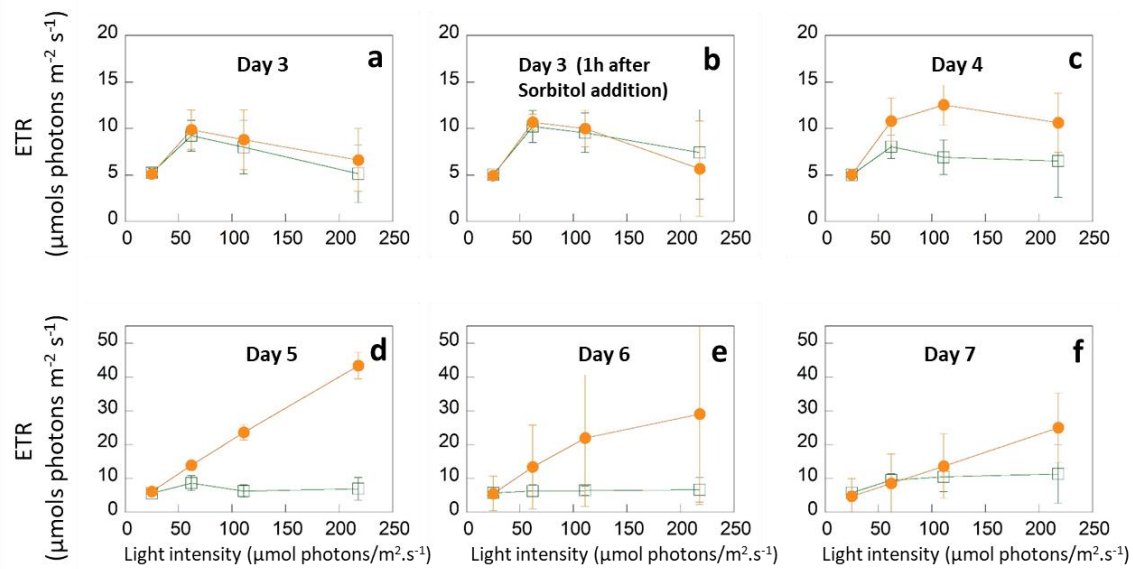
Figure S4: *In situ* **measurements of photosynthetic electron transfer rate (ETR) in photoautotrophic (light) and mixotrophic (light + 25 mM D-sorbitol)** *G. sulphuraria* **SAG21.92 cells.** Cells were inoculated at 3.5 x 10^6 cell mL^-1 and grown in the light (transmitted light 10 µmol photons m^-2 s^-1) and air for three days before D-sorbitol was added (mixotrophy, orange) or not (autotrophy, green). Light was increased every day to keep the transmitted light to a constant value of 10 µmol photons m^-2 s^-1. **a-f**, After three days of growth, ETR was followed every day directly on cultures within the photobioreactor, to avoid possible temperature stress. Data from 3 biological replicates ± S.D.
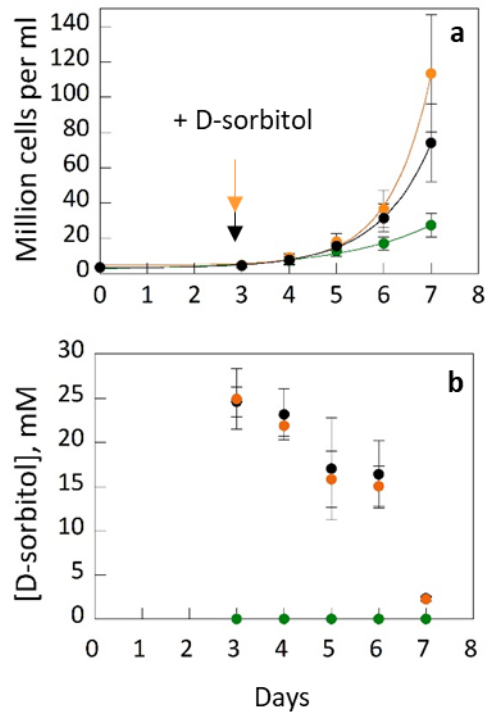
Figure S5: Enhancement of cell growth by mixotrophy and sorbitol consumption in *G. sulphuraria* SAG21.92. *G. sulphuraria* was inoculated at 3.5 10^6 cells mL^{-1}. At day 3, cultures were either continued without any addition (photoautotrophy, green), or supplemented with 25 mM D-sorbitol in the presence of light (mixotrophy, orange) or in the dark (heterotrophy, black). **a,** Growth curves (data from 12 biological replicates ± S.D.). Growth rates were 0.5 ± 0.1 day^{-1}; 1.2 ± 0.1 day^{-1} and 0.9 ±0.05 day^{-1} in photoautotrophic, mixotrophic and heterotrophic cultures, respectively. **b**, Sorbitol consumption in mixotrophic and heterotrophic cultures. Data from 3 biological replicates ± S.D.
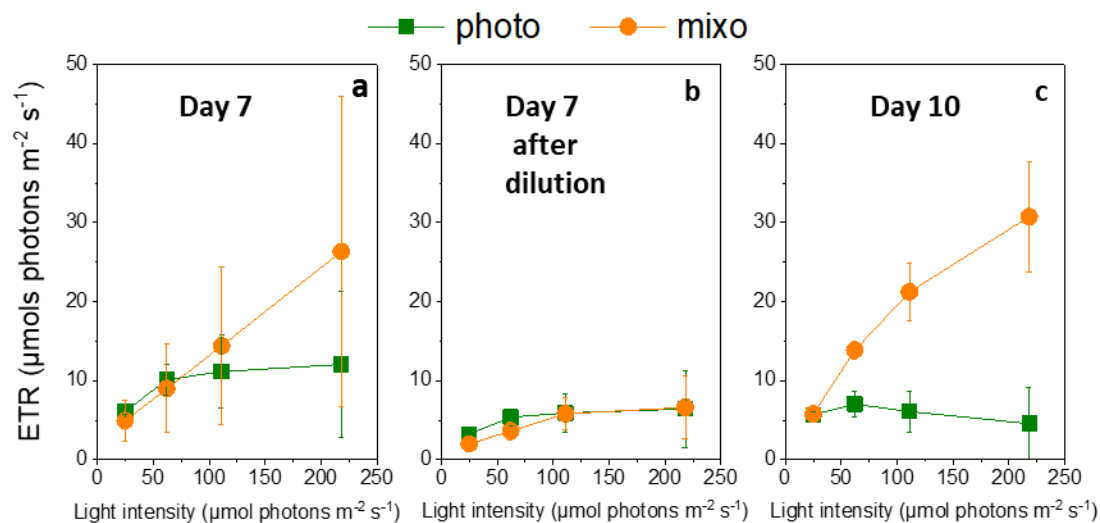
Figure S6: Mixotrophy is restored in *G. sulphuraria* SAG21.92 upon addition of a carbon source. a, Mixotrophic cells (orange) were let consuming sorbitol (day 7, *i.e.* 4 days after addition of D-sorbitol). **b,** Cells at day 7 were diluted to 3.5×10^6 cells mL^{-1}, and growth was resumed in the light (transmitted light 10 µmol photons m^{-2} s^{-1}) without D-sorbitol (photoautotrophy, green) or in the presence of 25 mM D-sorbitol (orange). ETR measurements carried three days later **(c)** indicate that mixotrophic photosynthetic capacity was fully restored. Data from 3 biological replicates ± S.D.
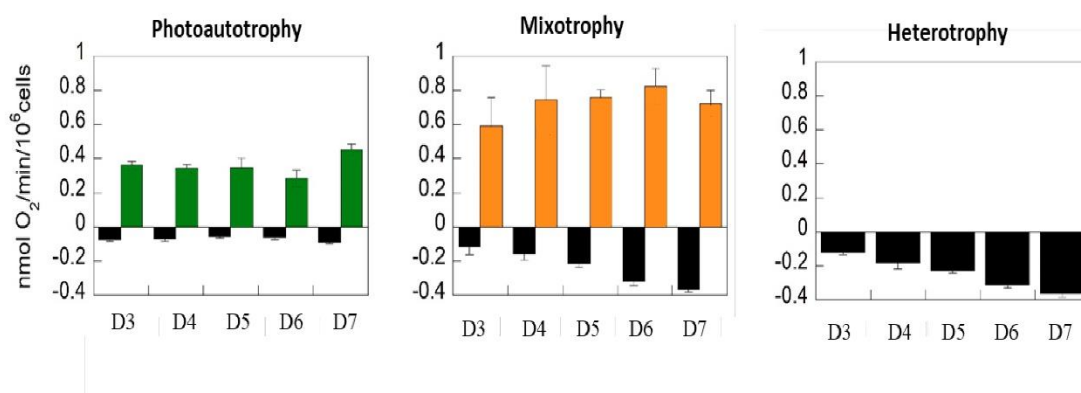
Figure S7: Respiration and net photosynthesis of *G. sulphuraria* SAG21.92 were measured every day in the three different growth conditions (photoautotrophy, mixotrophy and heterotrophy). O_2 consumption or production were measured with a Clark electrode at 42°C. Cells were centrifuged and resuspended at 3×10^7 cells in 1 mL of fresh 2xGS medium. Net photosynthesis corresponds to gross photosynthesis +|respiration|. Data from 3 biological replicates ± S.D.
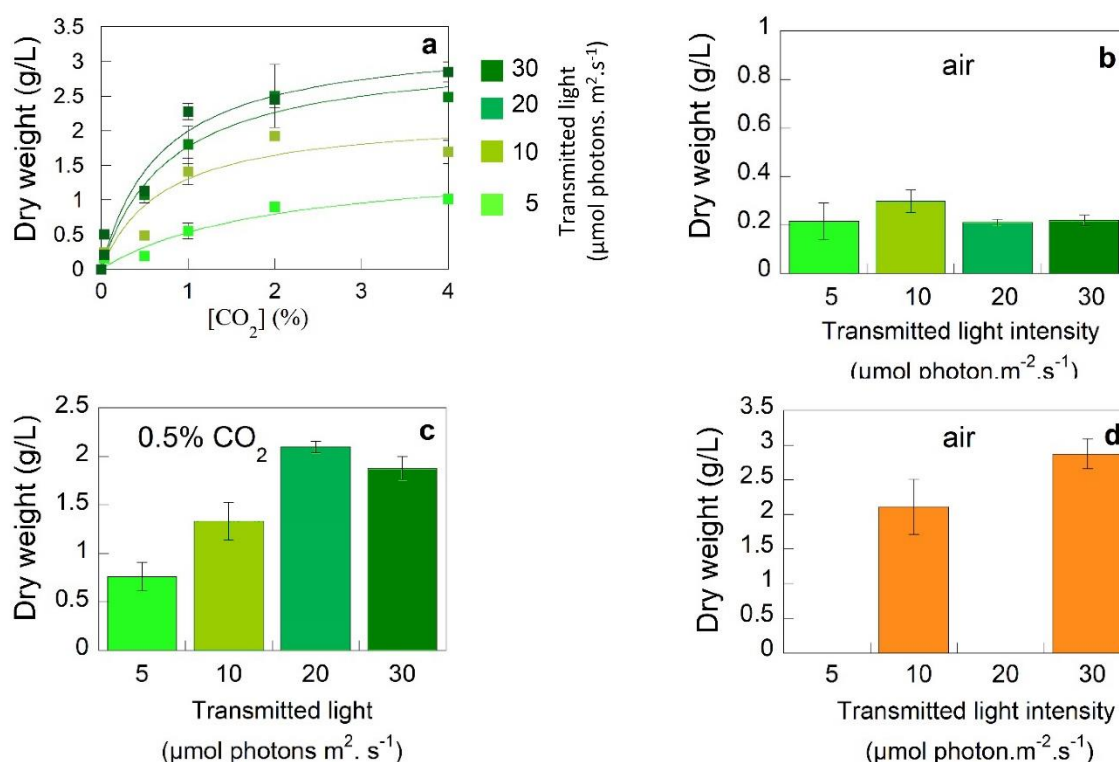
Figure S8: Biomass production of *G. sulphuraria* SAG21.92 as a function of transmitted light intensity and CO$_2$ concentration. a, Cells were grown in a photobioreactor at four different constant transmitted light intensities and different CO$_2$ concentrations. During growth, the light intensity was increased to maintain a constant transmitted light (from 5 to 30 µmol photons m^{-2} s^{-1}). Cells exposed to a given light ramp were used to inoculate the next experiment at higher CO$_2$ concentration, while repeating the same light ramp. Progressive adaptation to higher CO$_2$ concentration was chosen to avoid acidification of the cytosol in the presence of high CO$_2$ concentration and to induce a progressive reduction in the accumulation of carbonic anhydrase concentration, which is expected to be high in low CO$_2$ grown cells. After three days of adaptation, cells were grown for 4 additional days and collected at day 7, dried for three days at 60°C and weighted. Data from 3 biological replicates ± S.D. **b**: Focus on the light dependency of biomass production in phototrophic conditions in air. Same colour code as in panel a. Data from 3 biological replicates ± S.D. **c,** Focus on the light dependency of biomass production in phototrophic conditions supplemented with 0.5% CO$_2$. Same colour code as in panel a. Data from 3 biological replicates ± S.D. **d,** Focus on the light dependency of biomass production in mixotrophic conditions (sorbitol 25 mM). Two light intensities were tested corresponding to a transmitted light of 10 and 30 µmol photons m^{-2} s^{-1}. Data from 3 biological replicates ± S.D
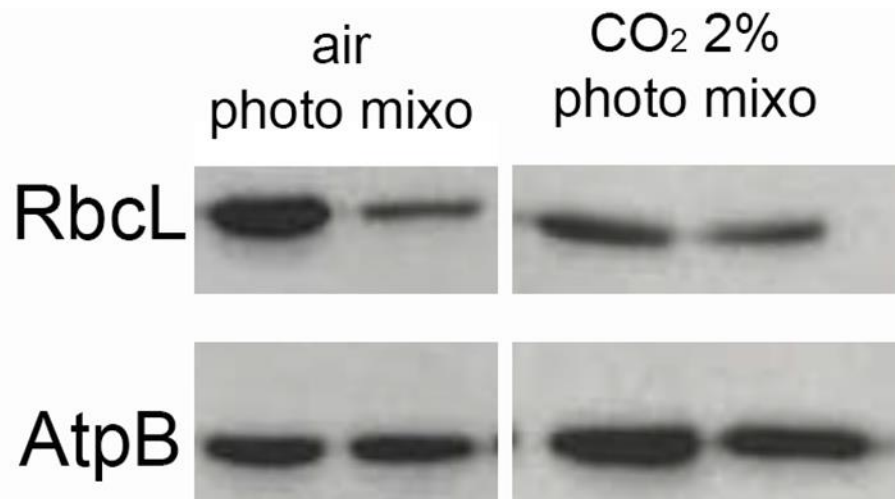
.

18

Figure S9: Immunodetection of RuBisCO in phototrophic and mixotrophic cultures of *G. sulphuraria* SAG21.92 under ambient and enhanced CO_2 atmosphere. Cells were grown in a photobioreactor in air ([CO_2]= 0.04 %) or air supplemented with CO_2. After 7 days of adaptation, cells were collected and broken with a Precellys homogeniser, through three cycles of 30 seconds at 10.000 rpm separated by a 30 seconds interval. Total protein extracts were analyzed by immunoblotting with anti- RuBisCO (AS03 037, Agrisera, Sweden). An antibody against the β subunit of the ATP synthase complex (AS05 085, Agrisera, Sweden) was used as a loading control. 10 µg of protein was loaded per well.
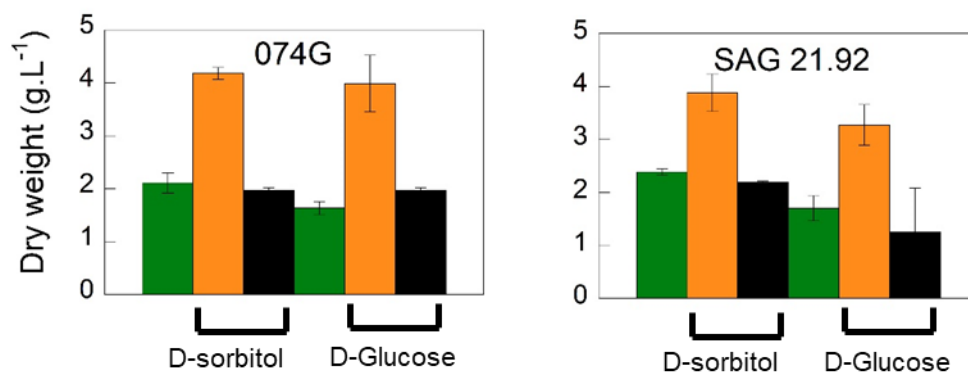
Figure S10: Comparative analysis of phototrophic (green), mixotrophic (orange) and heterotrophic (black) performances in *G. sulphuraria* 074 G and SAG21.92 species with D-sorbitol and D-glucose. *G. sulphuraria* 074 G and SAG21.92 species were grown in a photobioreactor as described in Fig. S3 & S4 under conditions similar to those described in Oesterhelt et al. (2007) in the presence of 2% CO_2 but at 42°C. At day 3 cells were either placed in the dark (black) in the presence of 25 mM D-sorbitol or D-glucose or exposed to light (transmitted light 10 µmol photons m^{-2} s^{-1}) in the absence of organic carbon (green) or in the presence of either 25 mM D-sorbitol or D-glucose as indicated in the graph. Cells were collected at day 7, dried and weighted. Growth performances of the 074G and SAG21.92 strains are very similar in the presence of D-glucose or D-sorbitol. Data from 3 biological replicates ± S.D.
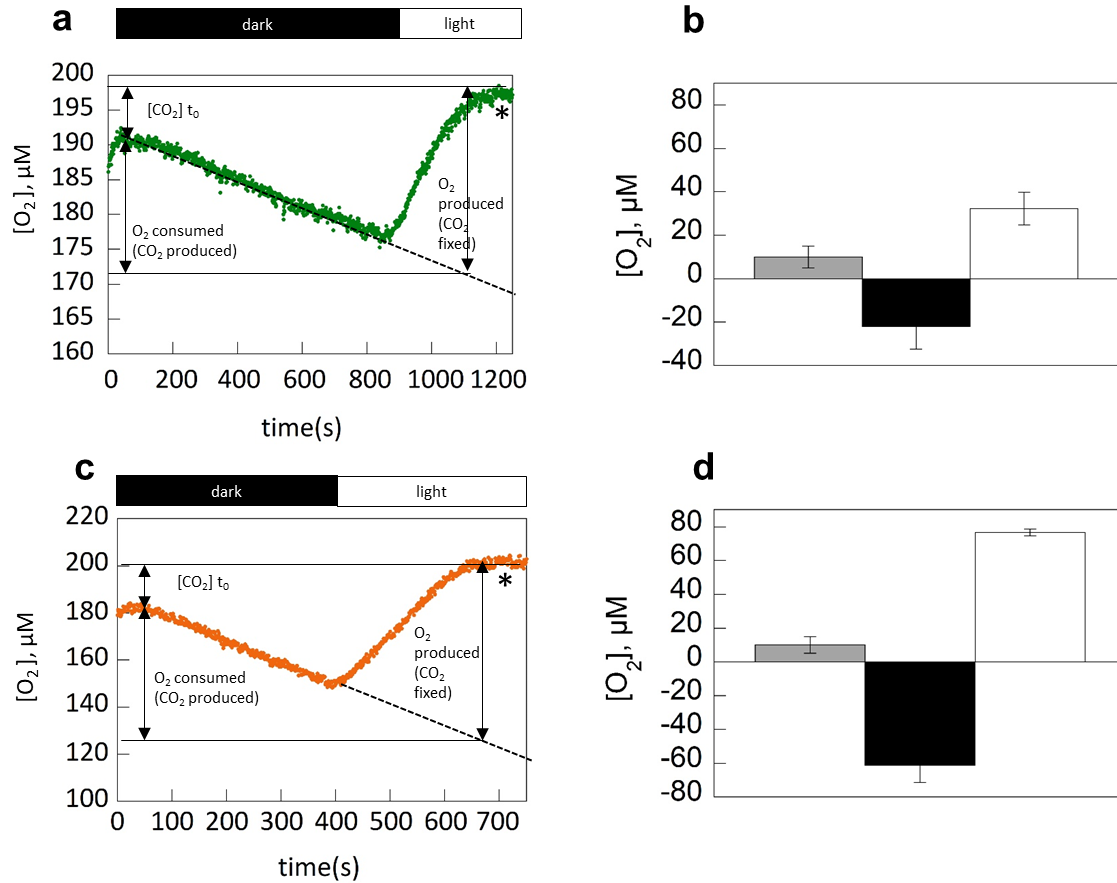
Figure S11: Respiration fuels photosynthesis in photoautotrophic (green) and mixotrophic (orange) *G. sulphuraria* **SAG21.92 cultures**. **a,c:** representative experiment of O_2 consumption or production measured in a closed system (Clark electrode) at 42°C. Photoautotrophic cells (a,b) or mixotrophic cells (c,d) were centrifuged and resuspended at $30 \cdot 10^6$ cells in 1 mL of fresh 2xGS medium. Stars indicate a dynamic equilibrium reached when all excess CO_2 from the media (CO_2 initially present plus CO_2 produced by respiration) is fixed. Thus, photosynthesis becomes limited by CO_2 production by respiration, leading to the compensation point. **b (photoautotrophic cells) , d (mixotrophic cells)**: the amount of O_2 produced by photosynthesis (white) is commensurate with the amount of CO_2 available to Rubisco, i.e. the sum of respiratory CO_2 (evaluated from O_2 consumption, assuming a 1/1 stoichiometry between CO_2 released and consumed oxygen, black) plus the small CO_2 amount initially present in the medium (10 μM *ca* at pH 2, grey), Data from 3 biological replicates ± S.D.
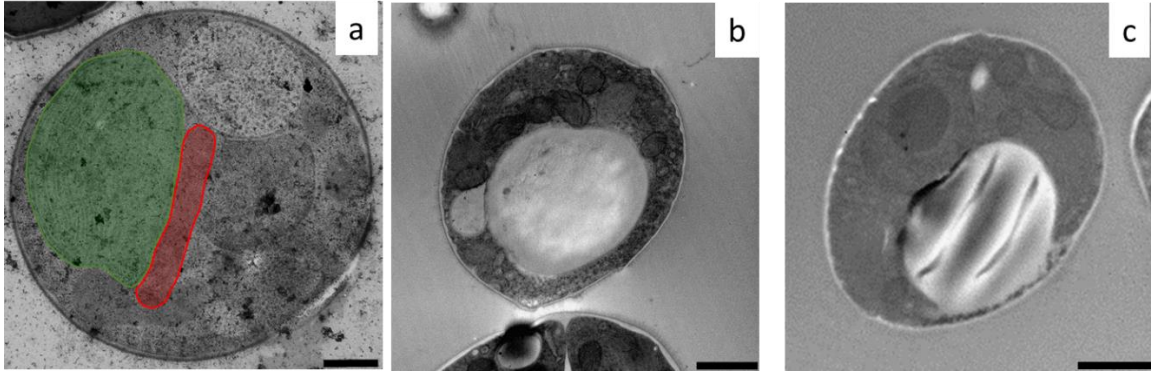
Figure S12: Transmission electron microscopy of *G. sulphuraria* SAG21.92 grown 5 days under photoautotrophic (a), mixotrophic (b) and heterotrophic (c) conditions. b, **c** show the presence of a huge floridean starch grain in the cytosol of the cells four days after addition of 25 mM D-sorbitol. Scale bars: **a**: 0.5 µm; **b**, **c**: 1 µm. In a, mitochondria and plastids are highlighted in red and green, respectively.

Dataset S1 (separate file). Proteins involved in photosynthesis, central metabolism and respiration were selected from the complete proteomic dataset (see Supplementary Dataset S2) and used to build Fig. 3. Proteins function and predicted localizations were checked manually (column "Manual annotation"). Cells highlighted in yellow in this column indicate proteins with statistically significant changes in abundance (see Threshold described in Supplementary Dataset S1). Blue-color and orange-color scales indicate decrease and increase in abundance, respectively (See Legend sheet).

Dataset S2 (separate file). Compared proteomic analysis between photoautotrophic, mixotrophic and heterotrophic growth conditions. Proteomics analyses were performed on biological triplicates for each growth condition. Quantification was obtained from extracting the MS1 intensity. Merging of results and filtering on both identification and quantification criteria as described in the Supporting Information resulted into 2100 proteins ("protein sets", sheet **Dataset S2-ALL**). These 2100 proteins were further divided into 694 proteins entirely missing in at least 1 condition (sheet **Dataset S2-MissingInOneCond.**) and 1406 proteins that have been quantified in all three conditions (in at least 1 replicate, sheet **Dataset S2-SeenInAllConditions**). This latter subset was submitted to differential analysis. Highlighted in blue : imputed values (in Dataset S2-SeenInAllConditions) that were assigned to partially missing abundance values (i.e. within one condition, in Dataset S2-ALL).

Dataset S3 (separate file). Compared metabolomic analysis between photoautotrophic, mixotrophic and heterotrophic growth conditions.
GC-MS sheet: In the table 32 compounds are listed with their retention time and chosen quantifier ion fragment. Compound identification was based on retention time and fragment pattern match with an in-house library or the NIST library. Peak areas of each compound were normalized to the internal standard and transformed to readable values by a multiplicator. The p-value for the sample group was calculated using the multiple comparison function from PRISM software based on

the Students t-test. **IC-MS sheet**: In the table 31 compounds are listed with their retention times and calculated molecular weights. Compound identification was based on 5 different sources of which the in-house database created with mzVault was the preferred source of identification. Batch normalization was carried out with pooled QC samples frequently measured during the batch. The p-value for the sample group was calculated in Compound Discoverer by running the Tukey HSD test (posthoc) after an analysis of variance (ANOVA) test and correction was performed by using the Benjamini-Hochberg algorithm for the false discovery rate.

Supporting information references

Allen GJ. 1959. Studies with *Cyanidium caldarium*, an anomalously pigmented chlorophyte. *Archiv für Mikrobiologie* **32**: S. 270-277.

Bouyssie D, Hesse AM, Mouton-Barbosa E, Rompais M, Macron C, Carapito C, de Peredo AG, Coute Y, Dupierris V, Burel A, et al. 2020. Proline: an efficient and user-friendly software suite for large-scale proteomics. *Bioinformatics* **36**(10): 3148-3155.

Cuaresma M, Janssen M, van den End EJ, Vilchez C, Wijffels RH. 2011. Luminostat operation: A tool to maximize microalgae photosynthetic efficiency in photobioreactors during the daily light cycle? *Bioresource Technol* **102**(17): 7871-7878.

Huber W, Von Heydebreck A, Sultmann H, Poustka A, Vingron M. 2002. Variance stabilization applied to microarray data calibration and to the quantification of differential expression. *Bioinformatics* **18**(Suppl 1): S96-104.

Johnson X, Vandystadt G, Bujaldon S, Wollman FA, Dubois R, Roussel P, Alric J, Beal D. 2009. A new setup for *in vivo* fluorescence imaging of photosynthetic activity. *Photosynthesis Research* **102**(1): 85-93.

Maxwell K, Johnson GN. 2000. Chlorophyll fluorescence - a practical guide. *Journal of Experimental Botany* **51**(345): 659-668.

Oesterhelt C, Schmalzlin E, Schmitt JM, Lokstein H. 2007. Regulation of photosynthesis in the unicellular acidophilic red alga *Galdieria sulphuraria. Plant Journal* **51**(3): 500-511.

Wieczorek S, Combes F, Borges H, Burger T. 2019. Protein-level statistical analysis of quantitative label-free proteomics data with ProStaR. *Methods in Molecular Biology* **1959**: 225-246.

Wieczorek S, Combes F, Lazar C, Gianetto QG, Gatto L, Dorffer A, Hesse AM, Coute Y, Ferro M, Bruley C, et al. 2017. DAPAR & ProStaR: software to perform statistical analyses in quantitative discovery proteomics. *Bioinformatics* **33**(1): 135-136.